

# Synthesis of new analogues of the siderophore piscibactin

---

**Andlovec, Karlo**

**Master's thesis / Diplomski rad**

**2024**

*Degree Grantor / Ustanova koja je dodijelila akademski / stručni stupanj:* **University of Zagreb, Faculty of Pharmacy and Biochemistry / Sveučilište u Zagrebu, Farmaceutsko-biokemijski fakultet**

*Permanent link / Trajna poveznica:* <https://urn.nsk.hr/urn:nbn:hr:163:167128>

*Rights / Prava:* [In copyright](#)/[Zaštićeno autorskim pravom.](#)

*Download date / Datum preuzimanja:* **2025-02-05**



*Repository / Repozitorij:*

[Repository of Faculty of Pharmacy and Biochemistry University of Zagreb](#)



**Karlo Andlovec**

**Synthesis of New Analogues of the Siderophore  
Piscibactin**

**DIPLOMSKI RAD**

Predan Sveučilištu u Zagrebu Farmaceutsko-biokemijskom fakultetu

Zagreb, 2024.

This thesis has been submitted to the University of Zagreb, Faculty of Pharmacy and Biochemistry. The experimental work was conducted at Centro Interdisciplinar de Química e Biología, Universidade da Coruña, under the expert guidance of prof. dr. Jaime Rodríguez González and under the supervision of prof. dr. sc. Valerije Vrčec.

*Me gustaría dar las gracias a mis directores del CICA, Jaime y Carlos por darme la oportunidad de desarrollar la parte experimental de esta tesis en A Coruña, así como por su ayuda en la elección del tema de interés. En especial, agradezco a Ana toda su ayuda durante mi estancia y por haber estado ahí para mí siempre que he necesitado ayuda.*

*Zahvaljujem mentoru prof. dr. sc. Valeriju Vrčeku na pruženoj prilici za izradu diplomskog rada na Zavodu za Organsku kemiju, kao i na ukazanoj pomoći kad god mi je bila potrebna.*

*Najveće zahvale upućujem obitelji i prijateljima na bezuvjetnoj podršci i ljubavi koju mi pružaju tijekom cijelog života. Bez vas ne bih bio tu gdje sam danas.*

## TABLE OF CONTENTS

<b>1. INTRODUCTION.....</b>	<b>3</b>
<b>1.1 FISHERY AND AQUACULTURE.....</b>	<b>3</b>
<b>1.2 BACTERIAL DISEASES IN FISH.....</b>	<b>4</b>
<b>1.3 THE ROLE OF IRON IN BACTERIAL DEVELOPMENT.....</b>	<b>5</b>
<b>1.4 SIDEROPHORES.....</b>	<b>6</b>
<b>1.5 MECHANISMS OF IRON UPTAKE.....</b>	<b>9</b>
<b>1.6 PISCIBACTIN.....</b>	<b>10</b>
<b>1.7 ANTIMICROBIAL RESISTANCE (AMR).....</b>	<b>11</b>
<b>1.8 DFT CALCULATIONS.....</b>	<b>12</b>
<b>2. AIM OF THE PROJECT.....</b>	<b>17</b>
<b>3. MATERIALS AND METHODS.....</b>	<b>18</b>
<b>4. RESULTS AND DISCUSSION.....</b>	<b>19</b>
<b>4.1 RETROSYNTHETIC ANALYSIS.....</b>	<b>19</b>
<b>4.2 EXPERIMENTAL PART.....</b>	<b>21</b>
<b>5. CONCLUSIONS.....</b>	<b>41</b>
<b>6. ABBREVIATION LIST.....</b>	<b>42</b>
<b>7. REFERENCES.....</b>	<b>44</b>
<b>8. SUMMARY/SAŽETAK.....</b>	<b>47</b>

**1. INTRODUCTION**

**1.1 FISHERY AND AQUACULTURE**

The fishery and aquaculture sector plays a crucial role in ensuring food security and livelihoods by offering sustainability, nutrition, income, and job opportunities to millions of individuals. Additionally, it contributes to economic growth through activities such as harvesting, processing, and marketing. In 2020, the combined production of fisheries and aquaculture reached a record high of 214 million tonnes, with aquatic animals accounting for 178 million tonnes and algae for 36 million tonnes. The total first sale value of aquatic animal production in 2020 was estimated at USD 406 billion, with aquaculture production contributing USD 265 billion to this figure (FAO, 2023).

In 2020, approximately 59 million individuals were employed in the primary sector of capture fisheries and aquaculture worldwide. The production from fisheries and aquaculture can serve various purposes, including direct human consumption, conversion into fishmeal and fish oil, and, to a lesser extent, other non-food applications. Aquatic foods play a vital role in enhancing nutrition and global food security by serving as a significant source of essential macronutrients and micronutrients like vitamins, minerals (such as zinc, iron, iodine, and selenium), and omega-3 fatty acids. It makes up 7% of total animal protein intake (Figure 1). These nutrients are crucial in the diets of many nations, especially in regions where overall protein intake is low and individuals face nutritional deficiencies (FAO, 2023).

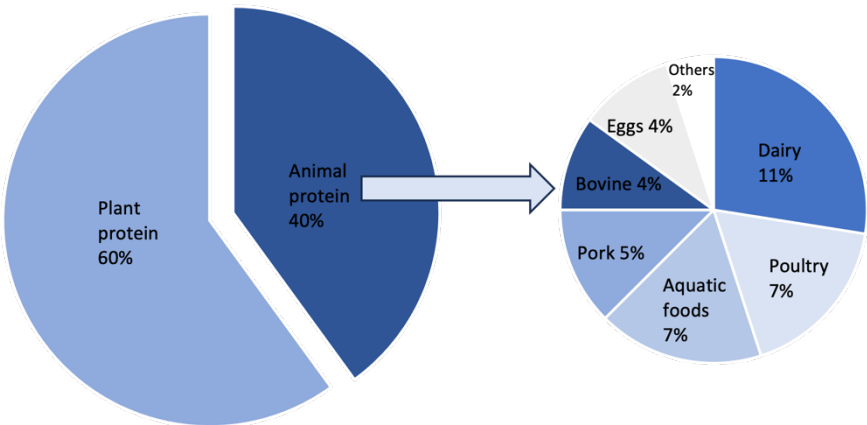


Figure 1. Contribution of plant and animal protein to global average daily protein intake (FAO, 2023).

Key factors in this industry are supply of raw ingredients for aquafeeds, reducing animal losses from disease outbreaks and ensuring the highest standards of food safety. (Norman et al., 2019).

As per the Food and Agriculture Organization (FAO) of the United Nations, wild fishing has remained stable over the past two decades, while global aquaculture production has increased by over five times in the last thirty years. The rise in production heightens the risk of pathogen outbreaks and the development of infectious diseases, resulting in significant economic repercussions (de la Fuente et al., 2021).

## 1.2 BACTERIAL DISEASES IN FISH

The bacterium *Photobacterium damsela* subsp. *piscicida* is the causative agent of fish pasteurellosis, also known as photobacteriosis or pseudotuberculosis, following taxonomic changes. This disease leads to significant economic losses in marine aquaculture on a global scale. Since 1990, it has been the primary pathological concern in the farming of sea bream and sea bass in Mediterranean countries. As a Gram-negative bacterium, it is recognized as one of the most destructive bacterial pathogens in marine aquaculture due to its widespread presence, diverse host range, and high mortality rates. Key virulence factors of this pathogen include a plasmid-encoded apoptotic toxin, a polysaccharide capsular layer, and the ability to extract iron from its host (Souto et al, 2012).

*Vibrio anguillarum* is a bacterium commonly found in marine environments and is recognized as one of the primary pathogens in the global aquaculture sector. It is responsible for causing vibriosis, a severe haemorrhagic septicaemia that impacts both warm- and cold-water fish species of significant economic value. The virulence factors associated with *V. anguillarum* include those linked to chemotaxis, motility, adhesion, invasion, the secretion of extracellular enzymes, and various iron uptake mechanisms (Balado et al., 2018).

Yersiniosis is a disease caused by the bacterium *Yersinia ruckeri*, impacting a wide range of fish species globally, with salmonids being particularly vulnerable. Infected organisms typically do not exhibit specific symptoms, but changes in behaviour are commonly observed, including swimming near the surface, sluggish movements, reduced appetite, and haemorrhages around the oral cavity, body surface, and internal organs. Treatment options for this condition include antibiotics, immunostimulants, probiotics, and vaccines (Rodríguez Pedrouzo, 2023).

### 1.3 THE ROLE OF IRON IN BACTERIAL DEVELOPMENT

During the infectious processes, the virulence and survival of many bacteria depend on their capacity to compete efficiently for crucial nutrients within the host organism. Iron stands out as a vital micronutrient due to its involvement in essential enzymatic reactions, with its role in cellular redox chemistry being particularly significant. Its capability to coordinate and activate oxygen, along with possessing a reversible redox pair, Fe(II)/Fe(III), makes it highly suitable for catalysing a wide range of redox reactions and facilitating electron transfer processes (Segade Parado, 2015).

Despite its prevalence on Earth, the accessibility of iron is constrained due to its presence as Fe(III) at physiological pH, having very low solubility ( $K_{ps} = 10^{-39}$ ), making it unusable for microorganisms. Additionally, during infections, many bacteria face an iron-deficient environment, as the free iron levels in biological fluids typically hover around  $10^{-18}$  M; a phenomenon referred to as nutritional immunity (Segade Parado, 2015).

Nutritional immunity refers to the mechanism through which a host organism retains trace minerals to restrict pathogenic activity during an infection. During inflammation linked to infection, levels of minerals like iron and zinc in the bloodstream decrease rapidly and significantly. This reduction in iron and zinc is believed to deprive invading pathogens of these vital nutrients, thereby curbing the advancement and severity of the disease.

Therefore, the ability to obtain iron from the host is one of the most important virulence mechanisms of bacterial pathogens (Hennigar and McClung, 2016).

Most bacteria require  $10^{-6}$  M (cytoplasmic concentration) for growth (de la Fuente et al., 2023).

To overcome this extreme unavailability of Fe(III), bacteria have designed several mechanisms to obtain it from the environment, such as extracting it from glycoproteins and haemoproteins, acquiring it in the form of Fe(II) which is more soluble than Fe(III), or producing siderophores (Segade Parado, 2015).

## 1.4 SIDEROPHORES

Siderophores are low molecular weight molecules (500-1500 Da), with a strong affinity and selectivity for  $\text{Fe}^{3+}$  ions, with which they form soluble complexes upon binding. These compounds are synthesized by a majority of bacteria and utilized to acquire  $\text{Fe}^{3+}$  from environments lacking in this essential element. Given the vital role of iron in bacterial growth and infection progression, the production of siderophores has been identified as a critical virulence factor enabling potentially pathogenic bacteria to initiate and sustain infectious processes (Rodríguez Pedrouzo, 2023).

Siderophores have demonstrated diverse applications in fields such as medicine, biotechnology, bioremediation, molecular imaging, plant growth enhancement, and various other areas (de la Fuente et al., 2023).

They may also exhibit additional biological functions crucial for bacterial development, including the transportation of metals other than iron, non-metals, sequestration of toxic metals for detoxification, protection against oxidative stress, molecular signalling (quorum sensing), and antibiotic activity. Understanding these functions has led to the exploration of numerous biotechnological applications in medicine, such as bioremediation and the creation of contrast agents for nuclear magnetic resonance imaging. Furthermore, siderophores and their derivatives have shown potential as antitumor agents due to the concept that elevated iron levels are associated with increased cancer incidence. Cancer cells require higher iron levels for rapid proliferation and growth compared to normal cells. By sequestering iron, both siderophores and their analogues can impede cancer cells from acquiring iron, thereby inhibiting their proliferation and growth (Rodríguez Pedrouzo, 2023).

One of the most significant applications of siderophores is in the development of new antimicrobials through the Trojan horse strategy. This approach leverages the iron uptake mechanisms of certain bacteria, which utilize specific siderophores, to enhance the delivery of antibiotics into the bacteria more effectively. To implement this strategy, a conjugate is prepared comprising a siderophore analogue serving as an entry vector into the bacteria, a known antibiotic or drug with antibacterial properties in its free form, and a spacer linking both components. When the siderophore fragment binds to  $\text{Fe}^{3+}$ , it is recognized by specific proteins in the pathogenic bacteria, facilitating the entry of the antibiotic attached to it into the cell. This method circumvents the low permeability of bacterial membranes, thereby increasing the



efficacy of the antibiotic. An example of this approach is cefiderocol (Figure 2), a siderophore cephalosporin substituted with a catechol, which represents the first antimicrobial drug approved by health authorities for treating infections in humans caused by aerobic Gram-negative bacteria following this strategy. (Rodríguez Pedrouzo, 2023).

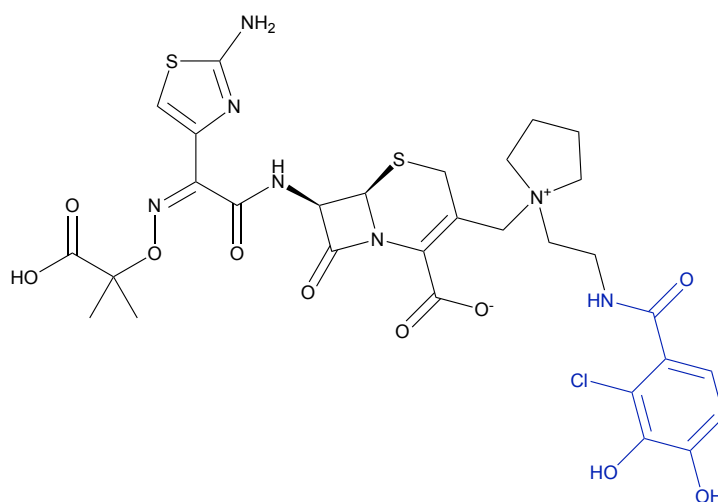
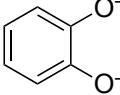
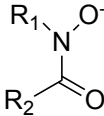
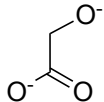
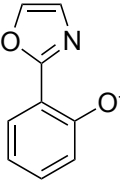
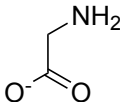
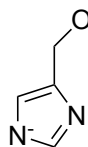


Figure 2. The structure of cefiderocol. The coloured part of the molecule represents a chloro-catechol benzoic acid derivative.

Siderophores possess functional groups containing electron-donating oxygen and nitrogen atoms, along with a structural configuration that enables them to function as hexadentate ligands, forming octahedral complexes with  $\text{Fe}^{3+}$ . The siderophore- $\text{Fe}^{3+}$  complexes in a high spin state exhibit exceptional thermodynamic stability (with a formation constant,  $K_f$ , exceeding  $10^{30} \text{ M}^{-1}$ ), showcasing their noticeable selectivity for  $\text{Fe}^{3+}$  over  $\text{Fe}^{2+}$  (Rodríguez Pedrouzo, 2023).

Siderophores exhibit a wide array of chemical structures, and their classification is based on the nature of the bidentate ligands present in their structure. They can be categorized into catecholates, hydroxamates,  $\alpha$ -hydroxycarboxylates, hydroxyphenyloxazolones,  $\alpha$ -aminocarboxylates, and  $\alpha$ -hydroxyimidazoles (as shown in Table 1), with catecholates, hydroxamates, and  $\alpha$ -hydroxycarboxylates being the most prevalent types. The pKa values associated with each type provide insight into their affinity for  $\text{Fe}^{3+}$  (Table 1). Additionally, mixed siderophores containing ligands of different types have also been observed (Rodríguez Pedrouzo, 2023).

Table 1. Classification of the most common siderophores according to their bidentate ligand and the according pKa values (Rodríguez Pedrouzo, 2023).

Type of ligand	Ligand structure	pKa
catechol		9.2, 13.0
hydroxamate		3.0, 14.5
$\alpha$ -hydroxycarboxylate		9.0
hydroxyphenyloxazolone		9.0
$\alpha$ -aminocarboxylate		2.5, 9.5
$\alpha$ -hydroxyimidazole		6.0, 14.5

Siderophores are typically produced by non-ribosomal peptide synthetases (NRPSs) or polyketide synthase (PKS) domains that collaborate with NRPS modules. A smaller portion of siderophores is also generated through pathways that do not involve NRPSs or polyketide synthases. The most common method of siderophore synthesis is through NRPSs, which involves a multi-enzyme assembly line. This process incorporates amino acids, carboxylic acids, and hydroxy acids into a peptide precursor molecule, which is then modified by NRPSs or other enzymes to form the final siderophore. One of these modifications includes the creation of heterocycles, such as the thiazoline ring formed by the cyclization of cysteine side chains. The secretion of siderophores is an energy-dependent process and is facilitated by efflux pumps, which are classified into different superfamilies based on the type of siderophore they transport (Kramer et al., 2020).

## 1.5 MECHANISMS OF IRON UPTAKE

The way in which iron-loaded siderophores are taken up differs between Gram-negative and Gram-positive bacteria (Kramer et al., 2020).

In Gram-negative bacteria, a common mechanism involves a  $\beta$ -barrel receptor in the outer membrane specifically recognizing the iron-loaded siderophore. Once the ligand binds to the receptor, it undergoes a conformational change, moving the iron-loaded siderophore into the periplasm. This process is supported by a TonB complex, which provides the necessary energy through the proton motive force. The iron-loaded siderophore is then transported into the cytosol, where iron reduction takes place, typically facilitated by an ATP-binding cassette transporter in the inner membrane. In some cases, the iron is reduced in the periplasm, and only the ferrous ( $\text{Fe}^{2+}$ ) iron is imported into the cytosol (Kramer et al., 2020).

In Gram-positive bacteria, no outer-membrane receptors are present, and siderophores are directly imported by ATP-binding cassette transporters that span the cell membrane. After releasing iron, some siderophores can be recycled through specific mechanisms, while others undergo hydrolysis to release iron (Kramer et al., 2020).

The synthesis, release, and uptake of siderophores are tightly regulated to maintain iron homeostasis within the cell. The key regulator is often Ferric uptake regulator (Fur), which acts as a transcriptional repressor of siderophore synthesis and an activator of regulatory proteins. When intracellular iron levels are sufficient, Fur binds to ferrous iron in the cytosol, blocking the transcription of siderophore synthesis genes or regulatory activator genes. Under iron limitation, Fur repression is lifted, leading to increased siderophore synthesis. Additionally, when iron-loaded siderophores enter the cell, extracytoplasmic function sigma factors or two-component systems act as checkpoints, triggering enhanced siderophore synthesis. This positive feedback loop signals to the cells that iron scavenging through siderophores is an effective strategy (Kramer et al., 2020).

Bacteria have the ability to produce multiple types of siderophores through biosynthesis. Depending on the environmental conditions such as temperature, pH, or the presence of other microorganisms, bacteria can choose to utilize one type of siderophore over another (Rodríguez Pedrouzo, 2023).

## 1.6 PISCIBACTIN

Piscibactin (Pcb) is a widespread siderophore produced by many species of bacteria (Lages et al., 2022). The isolation and characterization of Pcb, in its  $\text{Ga}^{3+}$  complex, were documented in 2012. It was first isolated from *Photobacterium damsela* subsp. *piscicida*. Pcb shares a close structural resemblance with siderophores such as pyochelin, yersiniabactin (Figure 3), and the antimycoplasma antibiotic micacocidin. It has been observed that Pcb is also produced by different species within the *Vibrio* genus. Notably, *V. anguillarum*, which causes vibriosis, not only produces Pcb, but Pcb also serves as a more significant virulence factor for fish infection compared to vanchrobactin, another siderophore produced by the same bacterium. Additionally, research indicates that the biosynthesis of both siderophores in *V. anguillarum* is regulated by iron levels and temperature (de la Fuente et al., 2021).

Pcb is a phenolate-type siderophore, comprising two thiazoline and one thiazolidine rings, with five stereogenic centers.

The presence of the labile thiazolidine ring and the  $\beta$ -hydroxy-2,4-disubstituted  $\alpha$ -methylthiazoline fragment, which is sensitive to acidic conditions, may account for the relatively low stability of Pcb (Rodríguez Pedrouzo, 2023).

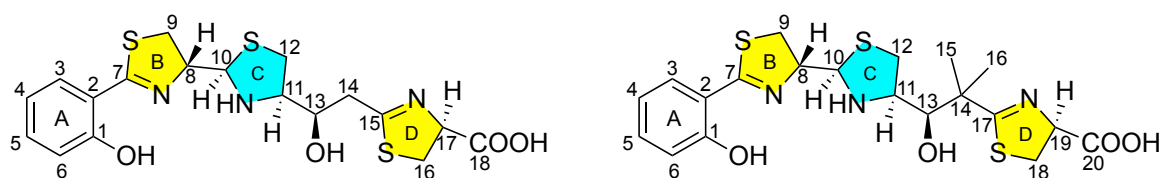


Figure 3. Structures of piscibactin (on the left) and yersiniabactin (on the right) with labelled rings and numbered carbon atoms.

## 1.7 ANTIMICROBIAL RESISTANCE (AMR)

The impact of antimicrobial resistance (AMR) goes beyond clinical medicine. It has wide-ranging effects on healthcare systems, economies, and patient outcomes worldwide. According to the World Health Organization (WHO), AMR is responsible for approximately 700,000 deaths each year (Al-Tawfiq et al., 2023).

Due to the global and escalating threat posed by antibiotic resistance, it is crucial to first comprehend the genetic foundation of bacterial resistance. Antibiotic resistance is commonly classified as either intrinsic or acquired. Intrinsic resistance is a naturally occurring phenomenon that is not influenced by antibiotic exposure and is universally present within the genome of a specific group of bacteria or bacterial species. This form of resistance is typically mediated by chromosomal factors and can be anticipated based on the organism's identity. For example, all *Klebsiella pneumoniae* are inherently resistant to ampicillin, while all *Enterococcus faecium* and *faecalis* are resistant to cephalosporins. Gram-positive cocci exhibit resistance to aztreonam, and gram-negative bacilli are resistant to vancomycin. Traditional mechanisms of intrinsic resistance include the lack of outer membrane permeability, which stops antibiotics from entering or accumulating inside bacterial cells; the existence of nonspecific efflux pumps that expel antibiotics and other substances from within bacterial cells; or the absence of target sites necessary for the antibiotic to bind to, thereby preventing it from killing or inhibiting the bacteria even if it enters the cell (Morrison and Zembower, 2020).

Antimicrobial resistance can also be acquired, and this is typically the type of resistance that raises concerns in clinical practice when bacteria that were initially susceptible to antibiotics develop resistance. Several factors contribute to acquired drug resistance, with antibiotic overuse being the primary cause. Acquired resistance can occur in one of two ways: through bacterial gene mutations or by acquiring foreign DNA that carries resistance genes. Bacteria reproduce rapidly, leading to evolutionary changes through random genetic mutations that can occur relatively quickly. Exposure to antibiotics creates an evolutionary pressure on bacteria, providing a survival advantage for those bacteria that have acquired resistance mutations. Alternatively, bacteria can transfer genetic material from one cell to another through horizontal gene transfer (Morrison and Zembower, 2020).

Understanding the specific resistance mechanisms is crucial for creating effective therapeutic strategies, in addition to knowing the genetic basis of resistance. Morrison and Zembower, (2020) determined that there are four types of resistance mechanisms:

1. Decreased drug accumulation: this can occur through decreased outer membrane permeability or increased active efflux of drugs across the cell surface.
2. Drug inactivation or modification: this involves the production of enzymes that can destroy or alter the antibiotic, making it ineffective.
3. Alteration of target or binding sites: this includes changes to penicillin-binding proteins or ribosomal-binding proteins.
4. Alteration of metabolic pathways: for example, enterococci can absorb folic acid from the environment, allowing them to bypass the effects of sulfamethoxazole-trimethoprim.

## 1.8 DFT CALCULATIONS

The density functional theory (DFT) is a computational approach used to analyse the electronic and structural characteristics of molecular systems. DFT operates on the principle that a system's total energy is solely dependent on its electronic density, which is a function of spatial coordinates. This method is particularly valuable for investigating iron or gallium complexes, transition metals exhibiting diverse oxidation states and geometries (Rodríguez Pedrouzo, 2023).

To investigate the possibility of replacing the harder-to-obtain thiazolidine or thiazoline rings with oxazoline or oxazole rings, which are more stable, and to assess whether the ability to form complexes with  $\text{Fe}^{3+}$  or  $\text{Ga}^{3+}$  is maintained, various structural motifs are proposed for study through computational calculations.

The proposed methods include:

- a) using models with  $\text{Ga}^{3+}$  complexes instead of  $\text{Fe}^{3+}$  for analyses using NMR techniques once synthesized,

b) substituting the terminal thiazoline (ring D) in Pcb with a more stable thiazole ring (T), as demonstrated in the publication by Lages et al. (2022), showing that this substitution does not affect the formation of  $\text{Ga}^{3+}$  complexes,

c) replacing the thiazoline (TZ) as ring B of Pcb with thiazole (T), oxazole (O), and oxazoline (OZ),

d) replacing the thiazolidine (TD) as ring C of Pcb with thiazoline, oxazoline, oxazolidine (OD), and pyrrolidine (P) (Rodríguez Pedrouzo, 2023).

The proposed model structures shown in Figure 5 were used for computational calculations using density functional theory (DFT) to determine if these models have the ability to form octahedral complexes with  $\text{Ga}^{3+}$ .

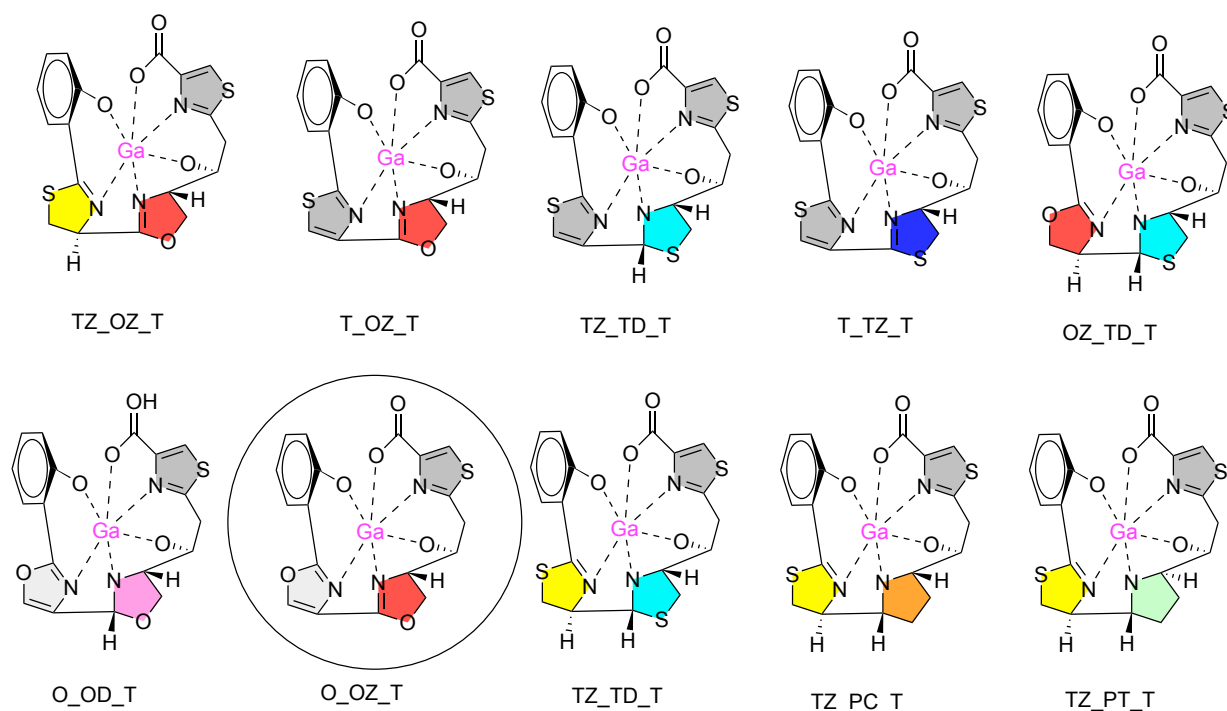


Figure 5. Proposed models of Pcb analogues coordinated with  $\text{Ga}^{3+}$ .

TZ: thiazoline, OZ: oxazoline, T: thiazole, TD: thiazolidine, O: oxazole, OD: oxazolidine, PC: pyrrolidine-cis, PT: pyrrolidine-trans.

The circled molecule is the goal product of this work.

To evaluate the capacity of each model to form  $\text{Ga}^{3+}$  octahedral complexes, two parameters were employed: the sum of the three transverse angles constituting the octahedron and the differences between the mean squares of the octahedron formed by two oxygen atoms and two

nitrogen atoms, and one nitrogen atom and another oxygen atom in the  $\text{Ga}^{3+}$  complex, assuming an ideal octahedral coordination sphere (Figure 6). The optimization of all proposed analogues enabled the assessment of the extent of distortion in the coordination sphere of the gallium atom with octahedral geometry (Rodríguez Pedrouzo, 2023).

While the transverse angles of an ideal  $\text{Ga}^{3+}$   $d2sp^3$  octahedral hybrid should be  $180^\circ$ , achieving this optimal structure is impossible because of the asymmetric distribution of the six coordinated atoms (three of oxygen and three of nitrogen) (de la Fuente et al., 2023).

Ideally, the sum of the transverse angles in the octahedral structure should be approximately  $540^\circ$  (three times  $180^\circ$ ), and any deviation from this value indicates the stability of the complex. Additionally, the difference between the sum of the Ga-heteroatom bond lengths for the N-Ga-N, O-Ga-N, and O-Ga-O configurations and the transverse distances between the N-N, O-N, and O-O heteroatoms offer insights into the degree of distortion in the octahedral structure. The sum of the transverse angles for the O-Ga-O, O-Ga-N, and N-Ga-N configurations in the DFT structures falls within the range of  $484\text{--}502^\circ$  (as shown in Table 2). The calculations conducted (as presented in Table 3) revealed average bond distances of  $1.96 \text{ \AA}$  for the Ga-O bond in O-Ga-O,  $2.05 \text{ \AA}$  for the Ga-N bond in O-Ga-N, and  $2.03 \text{ \AA}$  for the Ga-N bond in the N-Ga-N arrangements across all analogues, values that align well with similar gallium complexes documented in existing literature (Rodríguez Pedrouzo, 2023; Shakya et al., 2006; Padilha et al., 2017).

It is considered that the standard deviation (STD) of the difference between the transverse distance and the sum of the metal-heteroatom (N or O) distances in absolute value to be appropriate when it falls within the range of  $0.02\text{--}0.05$ , discarding it when it exceeds  $0.05$ . All proposed Pcb analogues exhibit angles and STD values suitable for good octahedral coordination with  $\text{Ga}^{3+}$  (Rodríguez Pedrouzo, 2023).



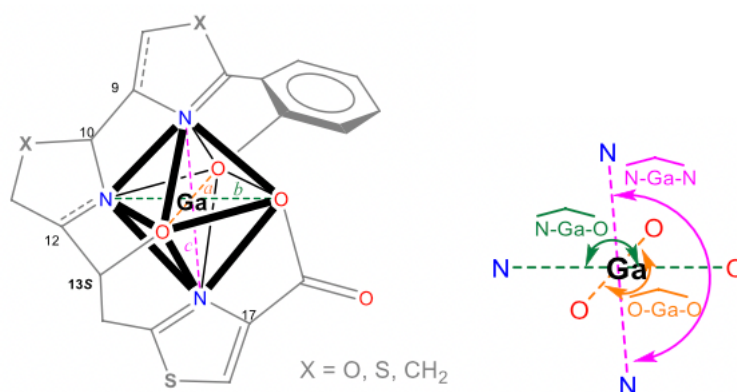


Figure 6. Model of Pcb analogues coordinated with  $\text{Ga}^{3+}$ , showcasing the octahedral structure of the complex (on the left) and the angles between atoms (on the right) (taken from Rodríguez Pedrouzo, (2023) with author's permission).

Table 2. Transverse angles in an octahedral environment, for the proposed Pcb analogues (Rodríguez Pedrouzo, 2023). The coloured row represents the goal product of this work.

Analogue	O-Ga-O	O-Ga-N	N-Ga-N	Sum
TZ_OZ_T	164.7	163.5	160.8	489
T_OZ_T	166	163	160	489
T_TD_T	166.9	170.1	160.5	497.5
T_TZ_T	165	162.2	159.8	487
OZ_TD_T	166.3	167.7	160.8	494.8
O_OD_T	166.8	165.3	157.4	489.5
O_OZ_T	166	160.2	158.4	484.6
TZ_TD_T	166.6	171	162.9	500.5
TZ_PC_T	166.3	171.1	164.4	501.8
TZ_PT_T	162.1	168.1	159.7	489.9

Table 3. Atom distances in the octahedral environment. Bond distances are displayed in angstroms (Å) (Rodríguez Pedrouzo, 2023). The coloured rows represent the goal product of this work.

Analogue	O-Ga-O	O-Ga-O	N-Ga-O	N-Ga-O	N-Ga-N	N-Ga-N
TZ_OZ_T	2,03	1,93	2,12	1,92	2,03	2,06
T_OZ_T	2,01	1,93	2,14	1,92	2,03	2,05
T_TD_T	2,01	1,9	2,21	1,91	1,99	2,05
T_TZ_T	2,02	1,92	2,14	1,92	2,02	2,05
OZ_TD_T	2,03	1,9	2,24	1,93	1,95	2,05
O_OD_T	2	1,9	2,28	1,92	1,97	2,04
O_OZ_T	2	1,92	2,21	1,93	1,99	2,04
TZ_TD_T	1,99	1,9	2,2	1,92	1,98	2,06
TZ_PC_T	1,99	1,9	2,13	1,93	1,97	2,06
TZ_PT_T	2,07	1,93	2,07	1,87	2,07	2,17

Analogue	O-O	N-O	N-N	$\Delta$ OO (a) <sup>1</sup>	$\Delta$ NO (b) <sup>1</sup>	$\Delta$ NN (c) <sup>1</sup>	STD <sup>2</sup>
TZ_OZ_T	3,93	4	4,03	0,03	0,04	0,06	0,04
T_OZ_T	3,91	4,01	4,01	0,03	0,05	0,07	0,05
T_TD_T	3,89	4,1	3,98	0,02	0,02	0,06	0,03
T_TZ_T	3,91	4,01	4,01	0,03	0,05	0,06	0,05
OZ_TD_T	3,9	4,15	3,94	0,03	0,02	0,06	0,04
O_OD_T	3,86	4,16	3,96	0,04	0,04	0,05	0,04
O_OZ_T	3,89	4,08	3,96	0,03	0,06	0,07	0,05
TZ_TD_T	3,86	4,1	3,99	0,03	0,02	0,05	0,03
TZ_PC_T	3,87	4,05	4	0,02	0,01	0,03	0,02
TZ_PT_T	3,96	3,92	4,16	0,04	0,02	0,08	0,05

<sup>1</sup> The difference between the transverse distance and the sum of the metal-heteroatom (N or O) distances (in absolute values). The colors in brackets correspond to the colors used in Figure 6.

<sup>2</sup> Standard deviation of  $\Delta$  values at input 1.

Based on the obtained results and the complexity of the synthetic path, it was decided to synthesize the oxazole-oxazoline-thiazole analogue (O\_OZ\_T), which shows suitable values for the two parameters mentioned earlier.

## 2. AIM OF THE PROJECT

The advancement in aquaculture and fish farming, leads to a consequent rise in bacterial infections in fish. These infections not only have a negative impact on the economy, but also pose a potential threat to human lives, as some infections can be transmitted to humans through the food chain (de la Fuente et al., 2021).

A small amount of free  $\text{Fe}^{3+}$  in the environment has resulted in competition among organisms, leading to various adaptations to ensure they obtain the iron necessary for growth and other biological functions. Additionally, there is a significant global issue of antimicrobial resistance that requires new solutions. One potential solution that emerges is siderophores, compounds with the ability to bind iron and with the potential of benefiting the aquaculture, the pharmaceutical industry, and the economy.

One such siderophore is piscibactin, a compound isolated from *Photobacterium damsela* subsp. *piscicida*. Piscibactin is inherently unstable, making it difficult to synthesize.

Through the use of DFT calculations, several potential analogues of piscibactin have been discovered that are chemically more stable, have a simplified structure, and exhibit strong chelation with iron and gallium, making them easier to synthesize. (de la Fuente et al., 2023).

The goal of this work is to synthesize an advanced intermediate in the synthesis scheme of a new analogue of piscibactin, which features an oxazoline and an oxazole ring, as well as only one chiral centre (Figure 4) instead of two thiazoline and a thiazolidine ring, along with five chiral centres present in Pcb. Starting from this compound, a new analogue could be prepared much more easily in the future.

The primary objective of this master's thesis project is to design a simplified analogue of Pcb that can chelate  $\text{Fe}^{3+}$  and is more stable than Pcb.

The goal is also to design a synthetic pathway for the intermediate, synthesize the mentioned compound, and characterize it using NMR, high-resolution MS, and TLC-MS techniques, achieving high yields and high purity compounds.

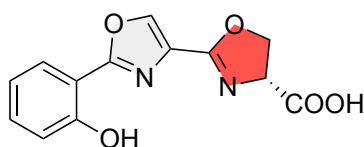


Figure 4. Structure of the compound 8 (goal molecule).

### 3. MATERIALS AND METHODS

The reactions that require anhydrous conditions were carried out under a dry, deoxygenated argon or nitrogen atmosphere. The solvents and anhydrous solutions were added to the reaction medium using a dry syringe. Reactions at 0°C were conducted using ice and water baths, and to reach even lower temperatures, a Cryocool-immersion CC-100 II cooling probe (Neslab) was used in an acetone bath. When necessary, reactions were heated using a stirring plate equipped with an aluminium heating block.

The dry CH<sub>2</sub>Cl<sub>2</sub> solvent was obtained by pre-drying and refluxing it over calcium hydride (CaH<sub>2</sub>), while in the case of DMF and THF, a commercially available extra dry 99.8% purity version, AcroSeal™ by ACROS Organics™, was used. The remaining solvents and reagents were used without purification.

The solvents were being evaporated using the rotary evaporator by Buchi; Rotavapor® R-200 and R-300, equipped with Waterbath B-480.

The reactions were monitored by thin-layer chromatography (TLC) using Merck silica gel GF-254 chromatography plates, which were visualized under UV radiation ( $\lambda=254$  nm). In some reactions where this method was not effective, TLC-MS was utilized, equipped with the CAMAG Interfase 2 module connected to a Bruker AmaZon speed Toxyper® spectrometer.

The purifications were done using medium-pressure column chromatography on silica gel (particle size 230-400 mesh, pore size 60 Å) from ACROS Organics™.

The nuclear magnetic resonance (NMR) characterization was carried out on a Bruker Avance 300 spectrometer with a NEO console (300 MHz for <sup>1</sup>H and 75 MHz for <sup>13</sup>C) at CICA

(Interdisciplinary Center for Chemistry and Biology). As deuterated solvents,  $\text{CDCl}_3$  (99.8% D) and  $\text{CD}_3\text{OD}$  (99.8% D) were used. NMR results were interpreted and analysed using MestReNova program.

Electrospray ionization (ESI) mass spectra were performed on a Thermo LTQ Orbitrap Discovery mass spectrometer at SAI (Research Support Service of the University of A Coruña).

The manufacturers of the used chemicals were: Sigma-Aldrich (for DAST and HOBt), Acros Organics (for EDCl, L-Serine methyl ester hydrochloride, DIPEA, DBU and  $\text{K}_2\text{CO}_3$ ), Euristop (for  $\text{CDCl}_3$ ), Activate Scientific (for D-Serine methyl ester hydrochloride), Alfa Aesar (for lithium hydroxide monohydrate), TCI (for  $\text{BrCCl}_3$ ), Fisher Chemical (for  $\text{MgSO}_4$ ) and MERCK-Schuchardt (for N-methylmorpholine).

As for the DFT calculations, conformational searches for each model were done using the MAESTRO software with a 5 kcal/mol energy window. DFT geometries were calculated using Gaussian 16 with the B3LYP/6-31G+(d,p) combination and an IEFPCM model for MeOH (Rodríguez Pedrouzo, 2023).

All the structures were drawn using Chemdraw program (22.2.0 version).

## 4. RESULTS AND DISCUSSION

### 4.1 RETROSYNTHETIC ANALYSIS

Retrosynthesis is a strategy that involves tracing back from the desired molecule to determine the initial components. Convergent synthesis requires creating essential fragments separately and subsequently merging them to produce the desired molecule, resulting in a higher overall yield and improved efficiency (Jabbar and Al-Hamashi, 2024).

For the design of the synthetic route, the retrosynthesis of the Pcb siderophore analogue is proposed (Figure 7). The thiazolidine C ring (TD) of a labile nature is replaced by a more stable oxazoline ring (OZ). The thiazoline B ring (TZ) is replaced by an oxazole one (O). Based on

preliminary studies, the terminal thiazole D ring (T) is maintained, and it confers greater stability to the structure (de la Fuente et al., 2023).

The 13S configuration of the hydroxyl group is necessary for its chelation with  $\text{Fe}^{3+}$  and  $\text{Ga}^{3+}$  (de la Fuente et al., 2023).

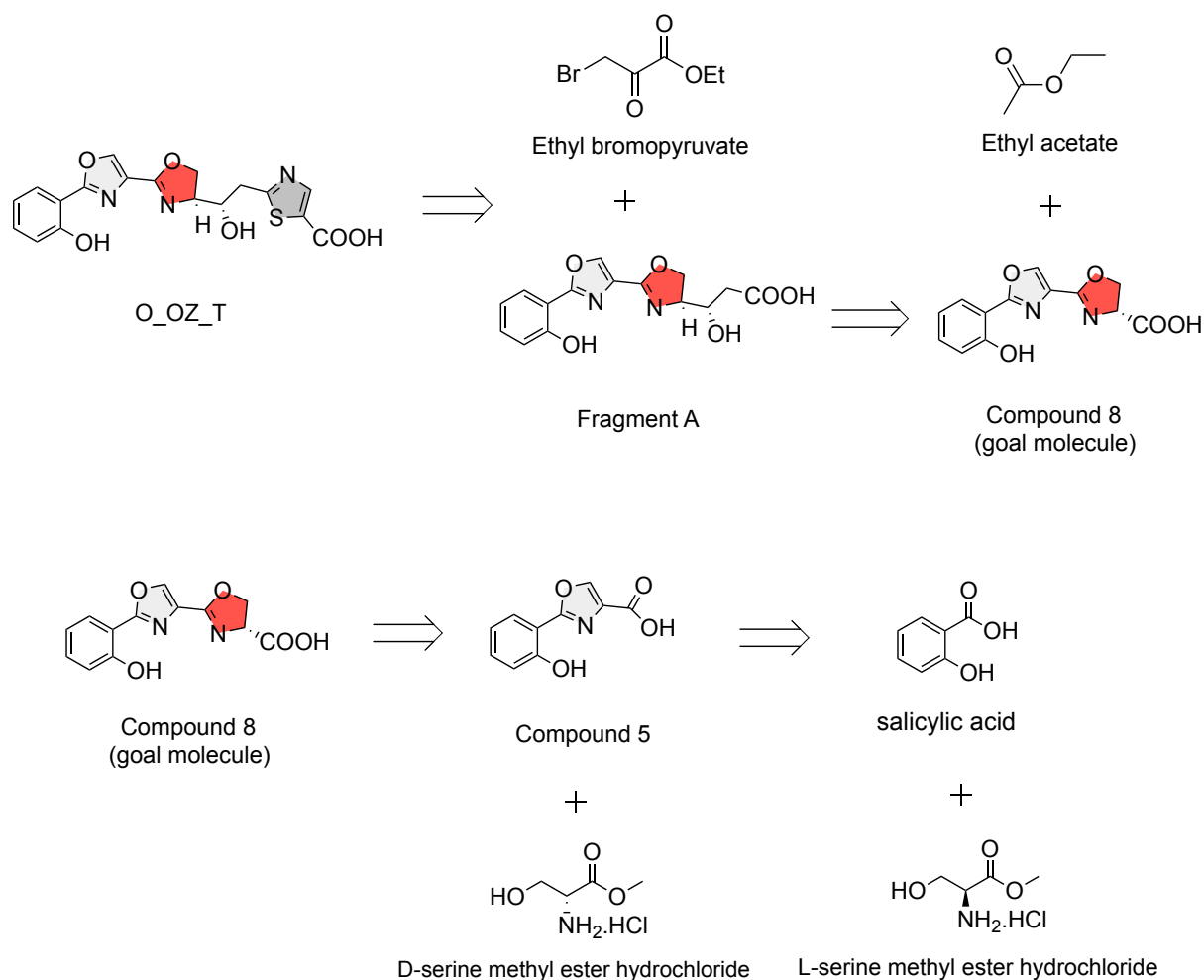


Figure 7. Retrosynthetic analysis for the preparation of the oxazole-oxazoline-thiazole (O\_OZ\_T) piscibactin analogue.

In the retrosynthetic analysis of the Pcb analogue O\_OZ\_T, the terminal thiazole ring would be obtained using the Hantzsch thiazole formation methodology from fragment A and ethyl bromopyruvate (Wu and Yang, 2013).

Fragment A would be formed by coupling between compound 8 and ethyl acetate. Furthermore, the oxazoline ring of compound 8 would be by coupling between compound 5 and D-serine

methyl ester hydrochloride. Finally, the oxazole of compound 5 would be formed by coupling between D-serine methyl ester hydrochloride and salicylic acid.

## 4.2 EXPERIMENTAL PART

### Synthesis of compound 1

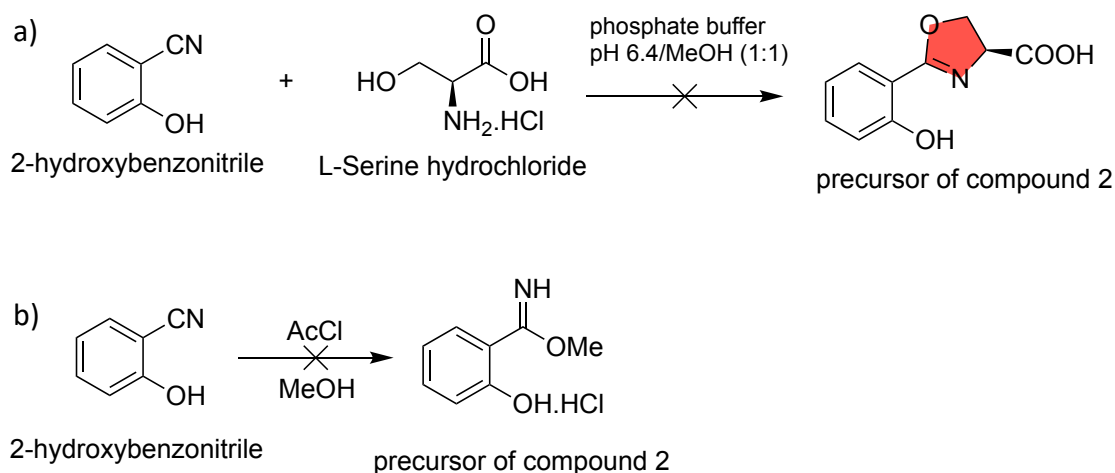


Figure 8. Unsuccessful attempts of synthesising a starting molecule.

The reactions a) and b) are showing the attempts of preparing the initial compound. The reaction similar to reaction a) was described by Segade Parado, (2015), but using a different amino acid (D-Cysteine instead of L-Serine). The reaction b) was described by Kaplan and Wuest, (2021). Both attempts were unsuccessful, resulting in low yield products and unexpected NMR signals, thus different route was chosen to prepare the starting compound.

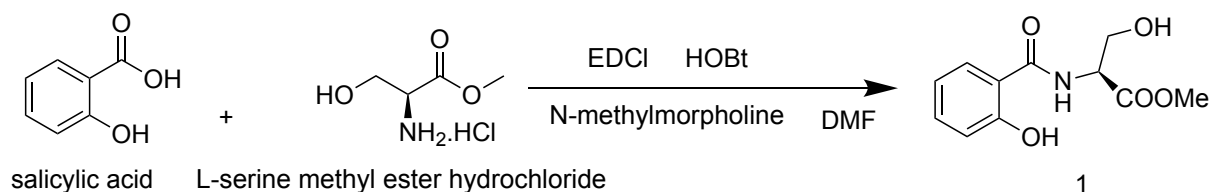


Figure 9. The synthetic route of compound 1.

In this reaction, salicylic acid and L-serine methyl ester hydrochloride form an amide bond in the process of amidation (Chan and Groves, 2021). The amine acts as a nucleophile, while the acid acts as an electrophile. EDC was used for activation of the acid and HOBt was used as a coupling additive, reducing racemization.

To the solution of salicylic acid (500.7 mg, 3.63 mmol), EDC.HCl (762.5 mg, 3.98 mmol) and HOBt.H<sub>2</sub>O (609.0 mg, 3.98 mmol) in 2 mL of anhydrous DMF, L-serine methyl ester (619.8 mg, 3.98 mmol) and N-methylmorpholine (440  $\mu$ L, 4 mmol) were added. The reaction was done using dry conditions and was being stirred for one hour at room temperature. Then the solvent was removed using the oil pump, after which the solid was partitioned between AcOEt and water (10 mL+10 mL). The water phase was then extracted with AcOEt (2 x 10 mL). The organic phases were combined, dried with MgSO<sub>4</sub>, filtered, and concentrated under reduced pressure. The product was then purified using the column chromatography: the column was first conditioned with 600 mL of AcOEt and hexane mixture (1:1); the purification started with 600 mL of 1:1 mixture and followed with 200 mL of AcOEt and hexane mixture (2:1), finishing with 200 mL of mixture (3:1). The fractions were combined and concentrated under reduced pressure, yielding **1** as a yellow oil (858.8 mg, 99%).

**<sup>1</sup>H NMR (300 MHz, CDCl<sub>3</sub>)  $\delta$  ppm:** 7.50 (d,  $J$  = 7.9 Hz, 1H, H3), 7.42 (t,  $J$  = 8.2 Hz, 1H, H5), 6.99 (d,  $J$  = 8.2 Hz, 1H, H6), 6.88 (t,  $J$  = 7.9 Hz, 1H, H4), 4.86 (dt,  $J$  = 7.0, 3.4 Hz, 1H, H8), 4.10 (qd,  $J$  = 11.2, 3.4 Hz, 2H, H9), 3.85 (s, 3H, H11).

**<sup>13</sup>C NMR (75 MHz, CDCl<sub>3</sub>)  $\delta$  ppm:** 170.75 (C, C10), 170.08 (C, C7), 161.64 (C, C1), 134.76 (CH, C5), 125.92 (CH, C3), 118.90 (CH, C4), 118.66 (CH, C6), 113.67 (C, C2), 63.16 (CH<sub>2</sub>, C9), 54.57 (CH, C8), 53.04 (CH<sub>3</sub>, C11).

**(+)-HRMS (ESI)  $m/z$ :** 262.0686 [M+Na]<sup>+</sup> (calculated for C<sub>11</sub>H<sub>13</sub>NNaO<sub>5</sub><sup>+</sup>: 262.0686).



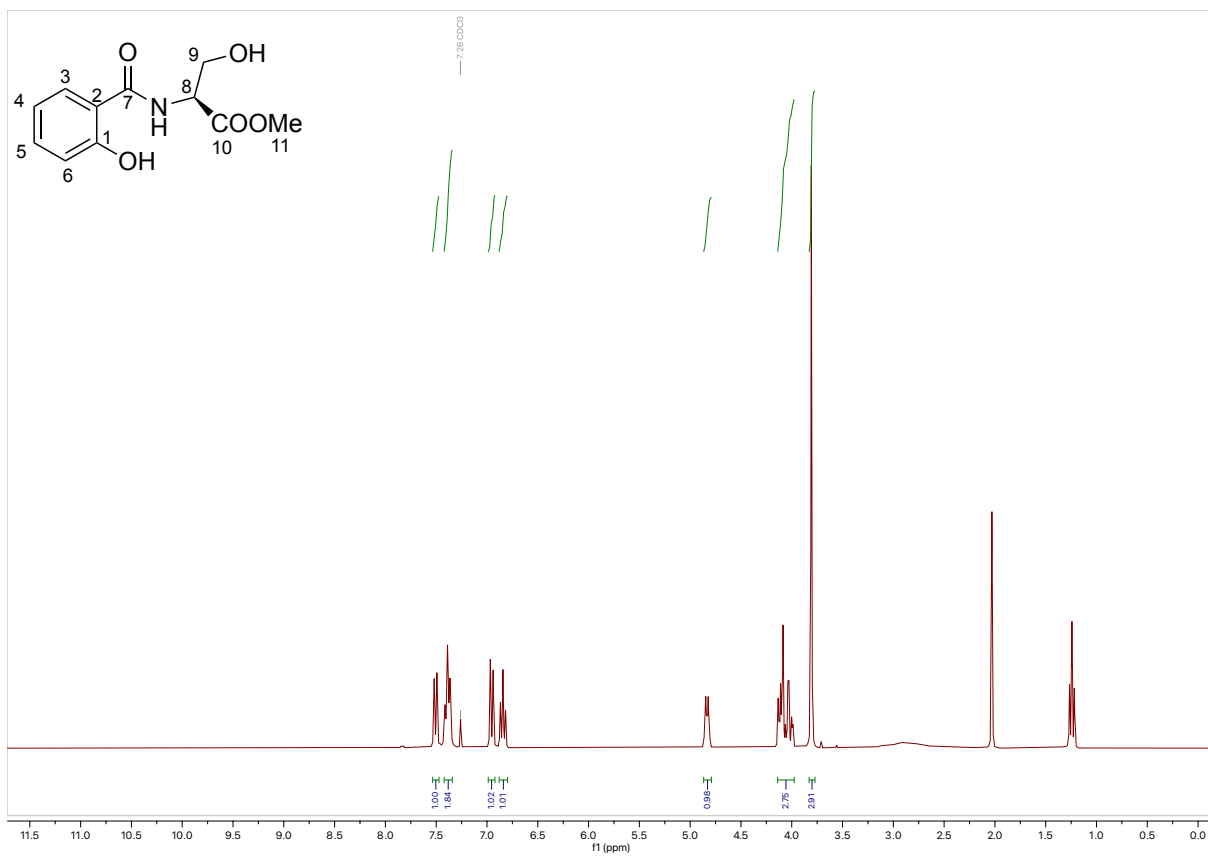


Figure 10. <sup>1</sup>H spectrum of compound 1 in CDCl<sub>3</sub>.

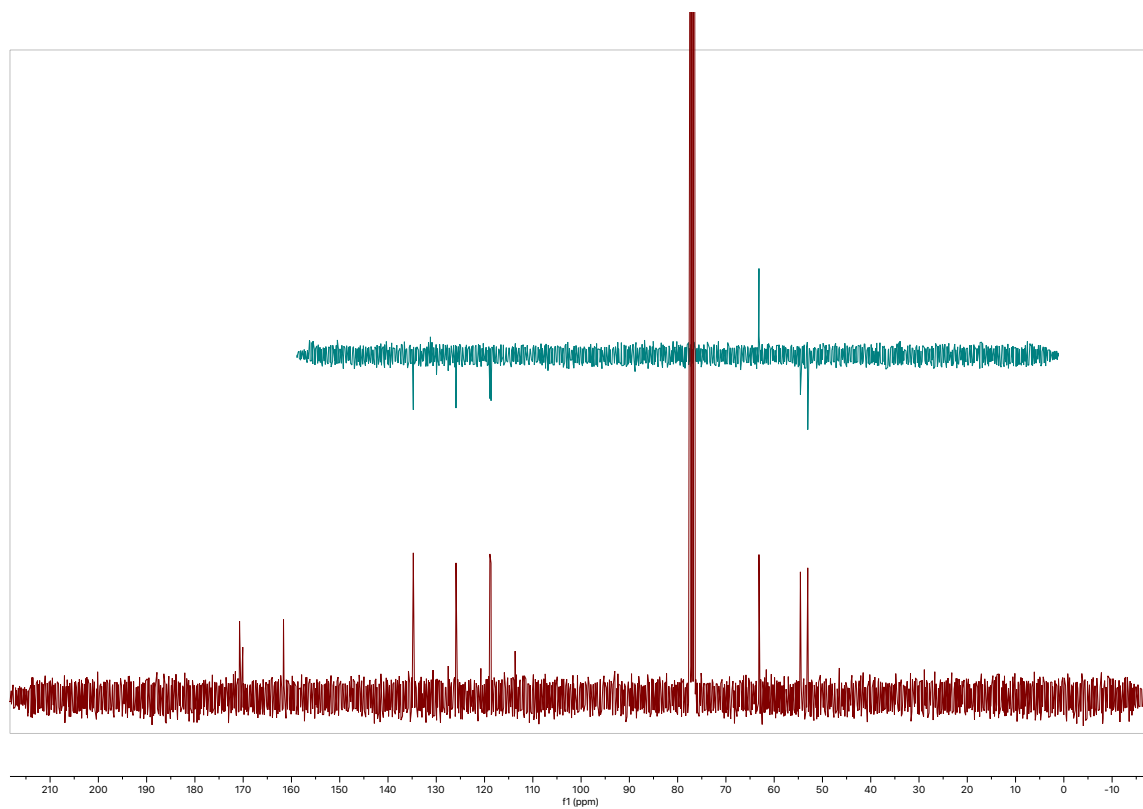


Figure 11. <sup>13</sup>C spectrum of compound 1 in CDCl<sub>3</sub>.

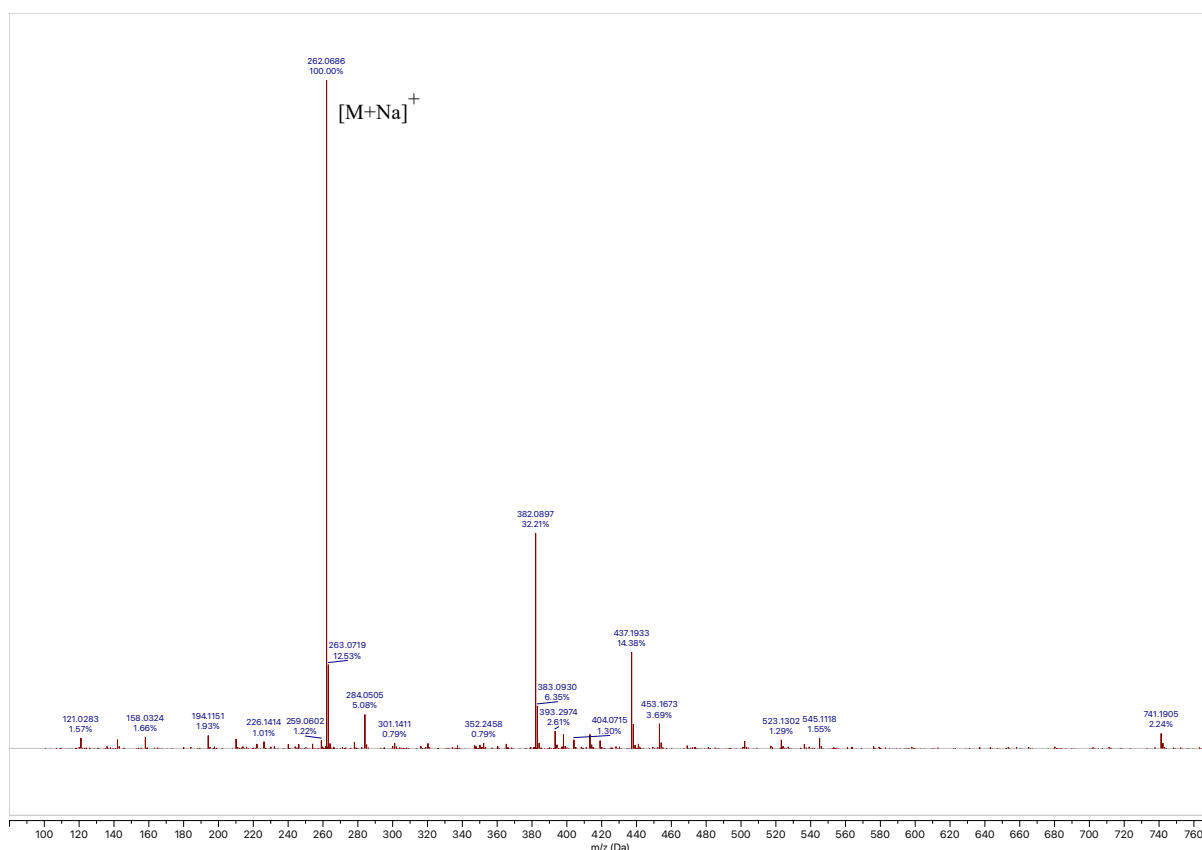


Figure 12. High-resolution MS spectrum of compound 1.

### Synthesis of compound 2

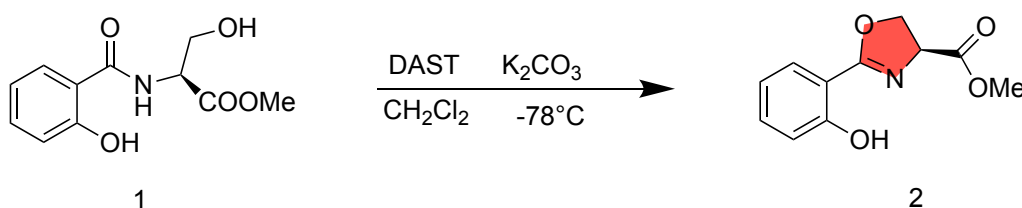


Figure 13. The synthetic route of compound 2.

Intramolecular cyclization and dehydration occur in this reaction, forming an oxazoline ring from molecule 1 (Chan and Groves, 2021). The reaction was promoted by DAST, otherwise known as a fluorinating agent. Cyclisation reactions using DAST are frequently carried out at reduced temperatures to regulate the reaction rate and enhance the selectivity of the desired product formation. Lower temperatures can prevent side reactions or the breakdown of reactants, resulting in a greater yield of the intended cyclised product. Furthermore, performing the reaction at lower temperatures can reduce impurity formation and enhance the overall efficiency of the cyclisation process (Chiotellis et al., 2014).

To the solution of compound **1** (469.0 mg, 1.96 mmol) in 10 mL of anhydrous CH<sub>2</sub>Cl<sub>2</sub>, DAST (320 μL 2.24 mmol) was added, and the reaction was being stirred for one hour at -78°C. After an hour, K<sub>2</sub>CO<sub>3</sub> (407.3 mg, 2.95 mmol) was added at room temperature to quench DAST. Then, 10 mL of saturated aqueous NaHCO<sub>3</sub> solution were added and the phases were separated. Aqueous phase was extracted with CH<sub>2</sub>Cl<sub>2</sub> (2 x 10 mL). The organic phases were combined, washed with 10 mL of saturated aqueous NaCl solution, dried with MgSO<sub>4</sub>, filtered, and concentrated under reduced pressure, yielding **2** as a light-yellow oil (376.0 mg, 87%).

**<sup>1</sup>H NMR (300 MHz, CDCl<sub>3</sub>) δ ppm:** 7.67 (d, *J* = 7.8 Hz, 1H, H3), 7.40 (t, *J* = 8 Hz, 1H, H5), 7.02 (d, *J* = 8 Hz, 1H, H6), 6.88 (t, *J* = 7.8 Hz, 1H, H4), 4.99 (dd, *J* = 10.5, 7.5 Hz, 1H, H8), 4.75 – 4.51 (m, 2H, H9), 3.81 (s, 3H, H11).

**<sup>13</sup>C NMR (75 MHz, CDCl<sub>3</sub>) δ ppm:** 170.98 (C, C10), 167.60 (C, C7), 159.97 (C, C1), 134.04 (CH, C5), 128.38 (CH, C3), 126.18 (C, C2), 118.82 (CH, C4), 116.96 (CH, C6), 68.92 (CH<sub>2</sub>, C9), 67.23 (CH, C8), 52.81 (CH<sub>3</sub>, C11).

**(+)-HRMS (ESI) *m/z*:** 244.0580 [M+Na]<sup>+</sup> (calculated for C<sub>11</sub>H<sub>11</sub>NNaO<sub>4</sub><sup>+</sup>: 244.0580).

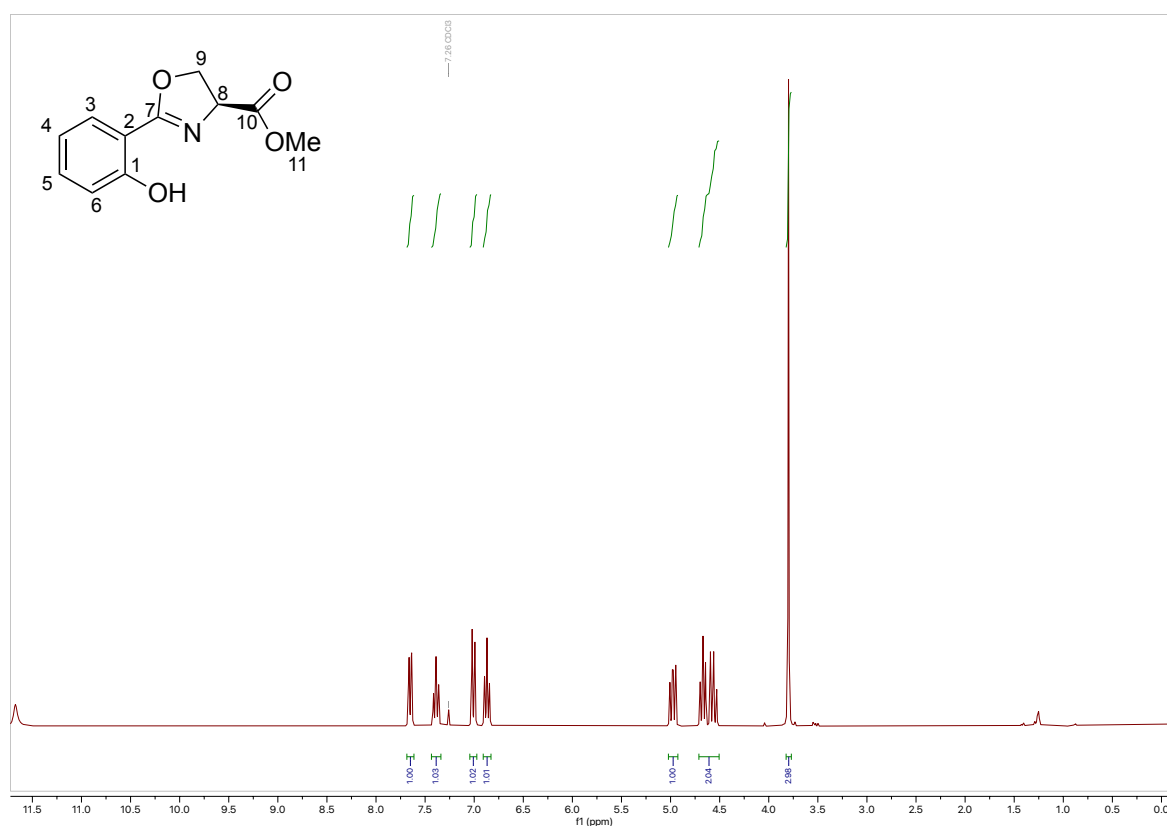


Figure 14. <sup>1</sup>H spectrum of compound **2** in CDCl<sub>3</sub>.

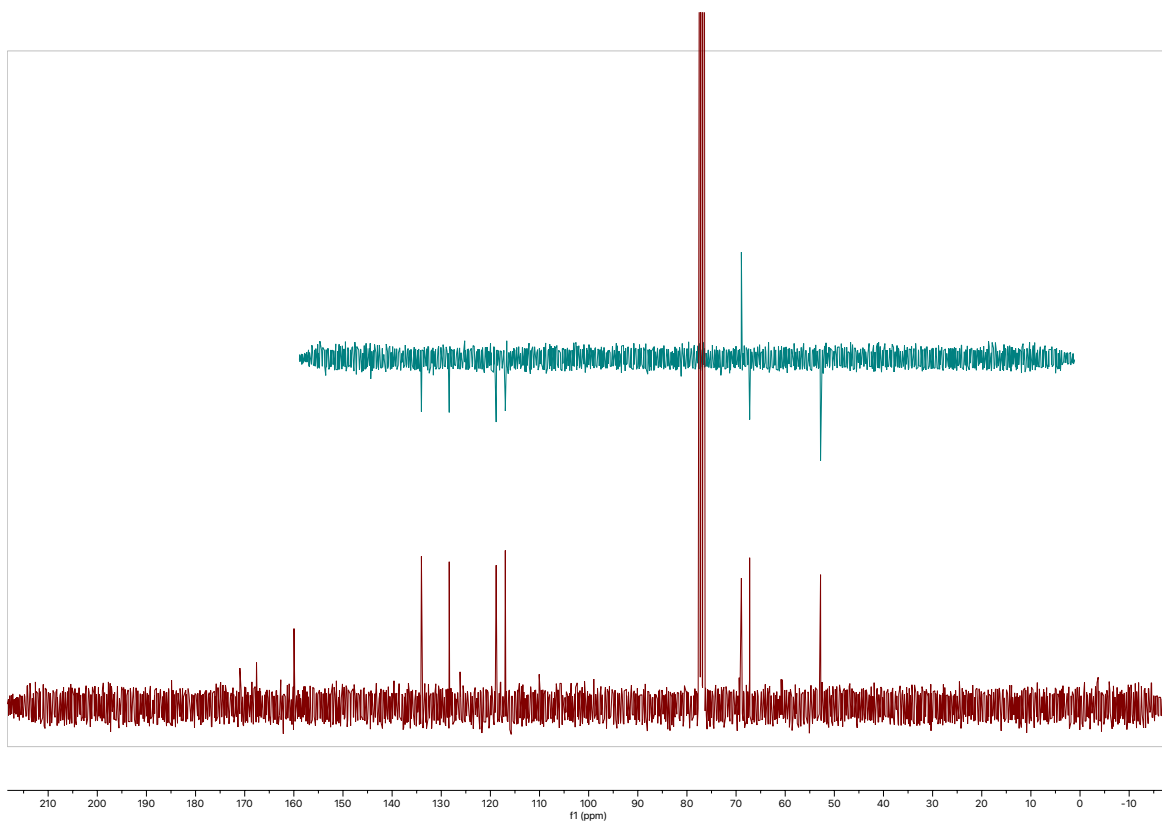


Figure 15.  $^{13}\text{C}$  spectrum of compound 2 in  $\text{CDCl}_3$ .

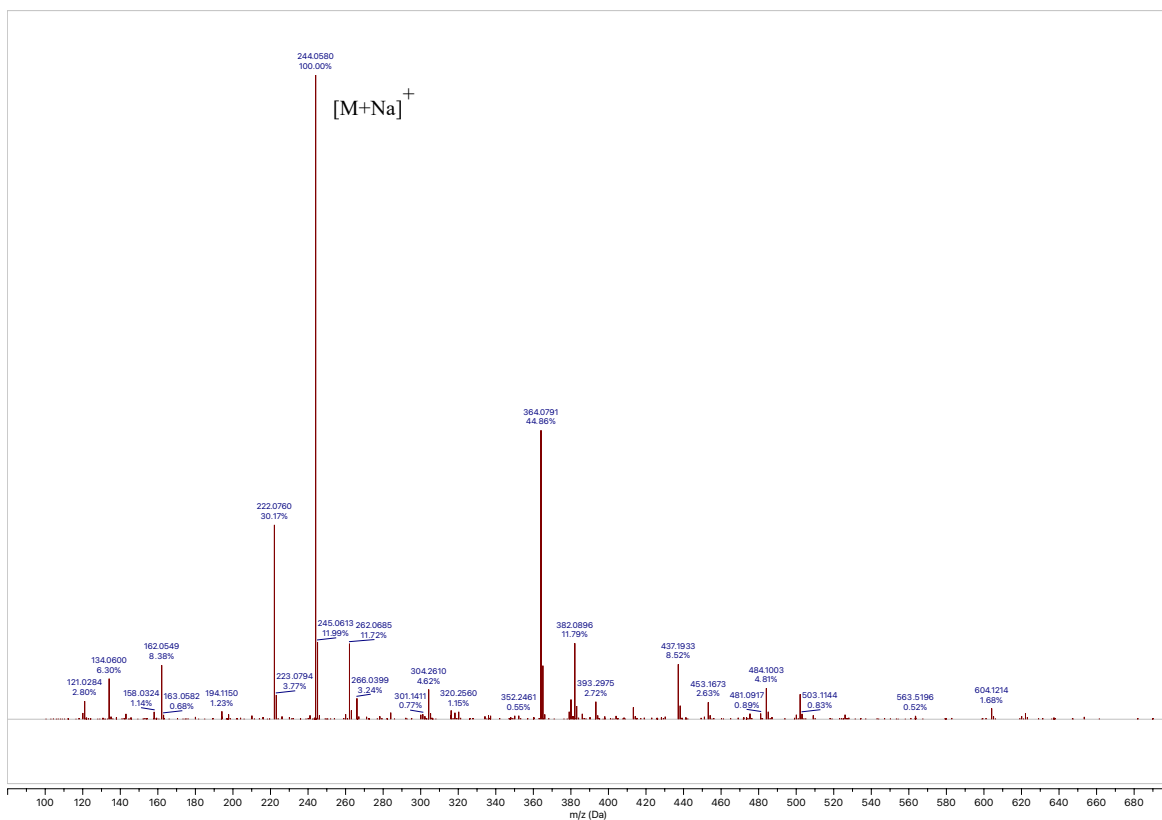


Figure 16. High-resolution MS spectrum of compound 2.

### Synthesis of compound 3

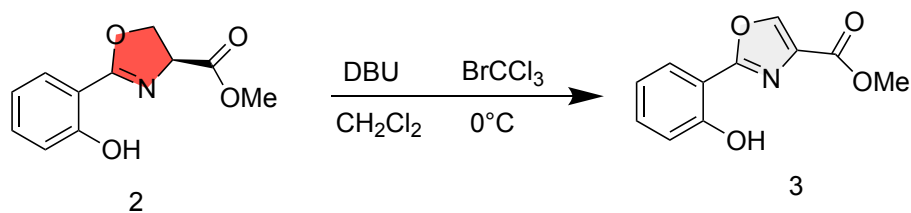


Figure 17. The synthetic route of compound 3.

In this reaction, oxidative aromatisation of oxazoline occurs, forming the corresponding oxazole (Kaplan and Wuest, 2021). One chiral centre is removed. DBU was used as a catalyst.

To the solution of compound **2** (275.5 mg, 1.25 mmol) in 10 mL anhydrous CH<sub>2</sub>Cl<sub>2</sub>, DBU (475 μL, 3.74 mmol) and BrCCl<sub>3</sub> (370 μL, 3.75 mmol) were added at 0°C. The reaction was being stirred for one hour at 0°C. After that, it was warmed to room temperature and washed with 10 mL of saturated aqueous NaHCO<sub>3</sub> solution, H<sub>2</sub>O, 0.05 M HCl, H<sub>2</sub>O and saturated aqueous NaCl solution. The organic phases were combined, dried with MgSO<sub>4</sub>, filtered, and concentrated under reduced pressure, yielding **3** as a yellow solidified product (272.9 mg, quantitative yield).

**<sup>1</sup>H NMR (300 MHz, CDCl<sub>3</sub>) δ ppm:** 8.25 (s, 1H, H9), 7.84 (d, *J* = 8 Hz, 1H, H3), 7.41 (t, *J* = 8.2 Hz, 1H, H5), 7.10 (d, *J* = 8.2 Hz, 1H, H6), 6.97 (t, *J* = 8 Hz, 1H, H4), 3.95 (s, 4H, H11).

**<sup>13</sup>C NMR (75 MHz, CDCl<sub>3</sub>) δ ppm:** 172.75 (C, C10), 170.96 (C, C7), 157.47 (C, C1), 142.43 (C, C9), 133.30 (C, C5), 126.28 (C, C3), 124.51 (C, C2), 119.61 (C, C4), 117.58 (C, C6), 110.12 (C, C8), 52.24 (C, C11).

**(+)-HRMS (ESI) *m/z*:** 242.0424 [M+Na]<sup>+</sup> (calculated for C<sub>11</sub>H<sub>9</sub>NNaO<sub>4</sub><sup>+</sup>: 242.0424).

In the literature by Kaplan and Wuest, (2021) the reaction was being stirred for one additional hour after warming the reaction to room temperature, but the product was already present and pure after only stirring for one hour at 0°C, thus it was decided not to stir the reaction for an additional hour.

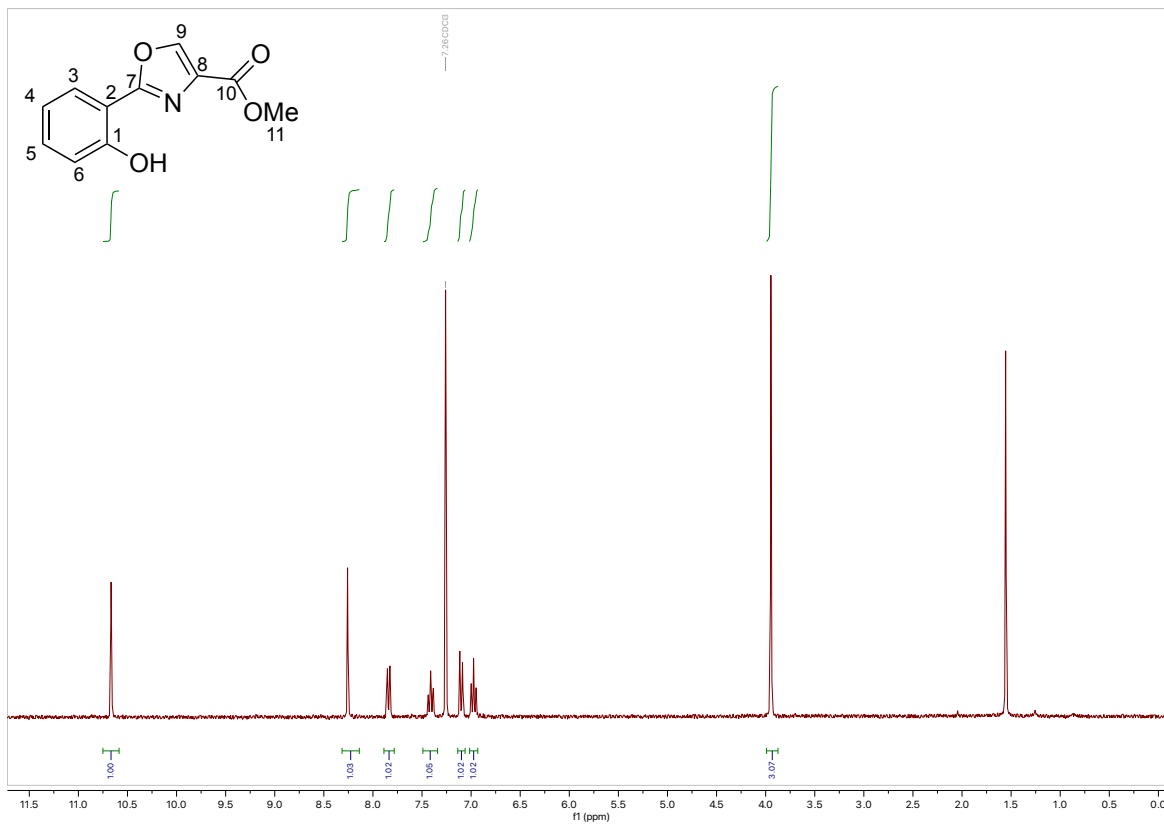


Figure 18. <sup>1</sup>H spectrum of compound 3 in CDCl<sub>3</sub>.

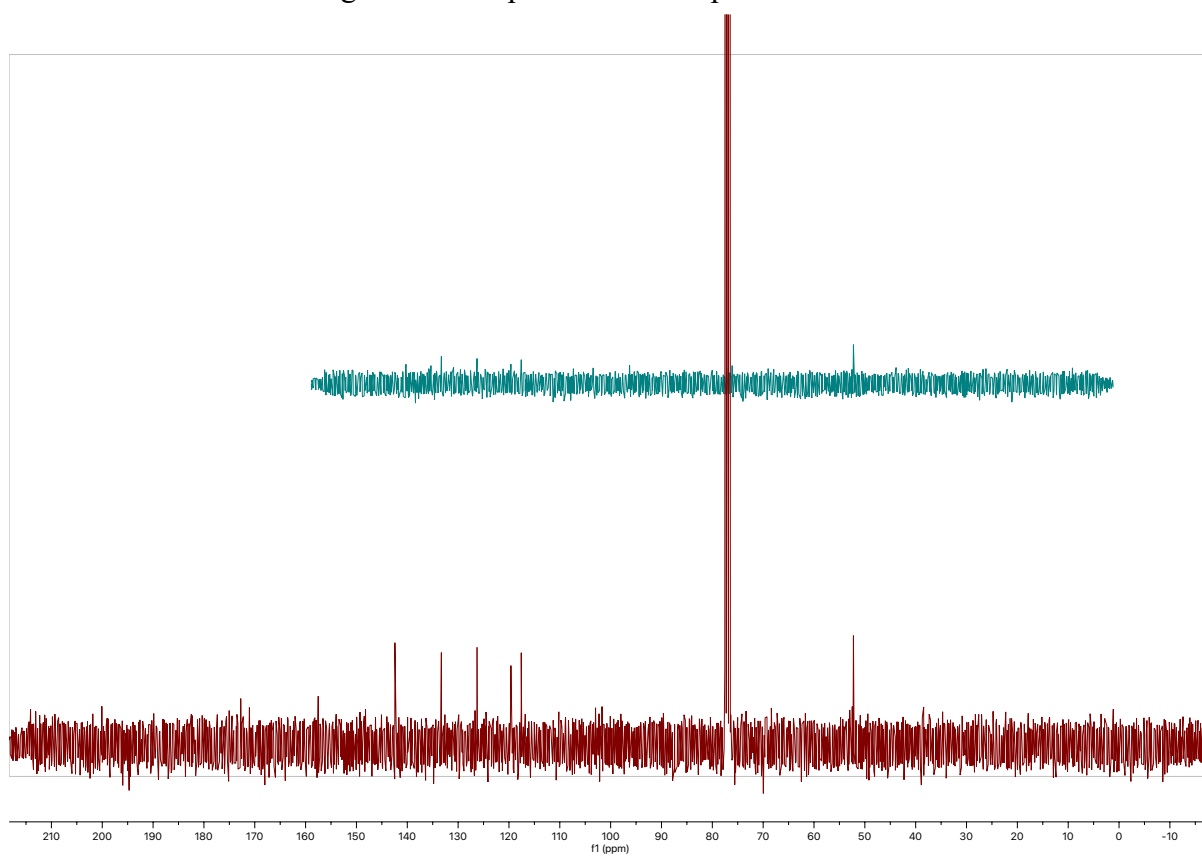


Figure 19. <sup>13</sup>C spectrum of compound 3 in CDCl<sub>3</sub>.

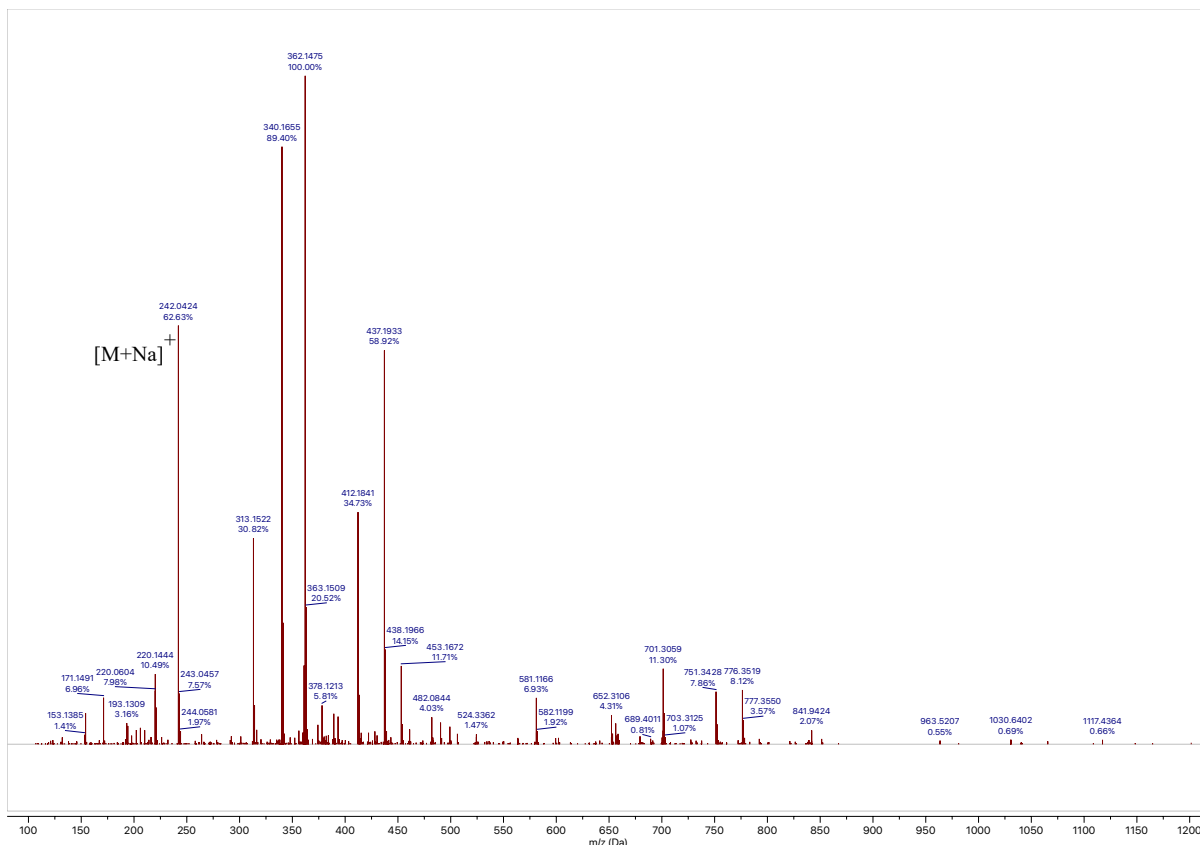


Figure 20. High-resolution MS spectrum of compound 2.

### Synthesis of compound 4

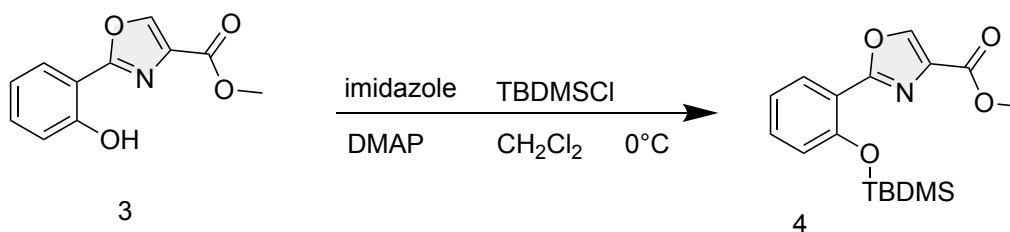


Figure 21. The synthetic route of compound 4.

This reaction shows an attempt of protecting the hydroxyl group using TBDMS (Li et al., 2023). The yield of the reaction was low, despite multiple tries and purifications which were conducted. NMR signals were not clean and were hard to interpret, hence it was decided to continue with the synthesis without the protected hydroxyl group.

To the ice-cold solution of compound **3** (39.5 mg, 180.2  $\mu\text{mol}$ ) in 10 mL of anhydrous  $\text{CH}_2\text{Cl}_2$ , TBDMSCl (106.0 mg, 0.7 mmol), imidazole (50.6mg, 0.74 mmol) and DMAP (4.2mg, 34.38  $\mu\text{mol}$ ) were added. The reaction was being stirred at room temperature and then 2 mL of DMF

were added to improve the solubility. The reaction was left to stir for 96 hours at room temperature. The solvent was then removed using the oil pump. The product was diluted with 10 mL of CH<sub>2</sub>Cl<sub>2</sub> and washed with 10 mL of H<sub>2</sub>O and 10 mL of saturated aqueous NaCl solution. The organic phase was dried with MgSO<sub>4</sub>, filtered, and concentrated under reduced pressure. The product was then purified using the column chromatography: the column was first conditioned with 100 mL of hexane; the purification started with 100 mL of hexane and followed with 100 mL of AcOEt and hexane mixture (1:4). The fractions were combined and concentrated under reduced pressure, yielding **4** as a light-yellow solidified product (24.9 mg, 41%).

### Synthesis of compound **5**

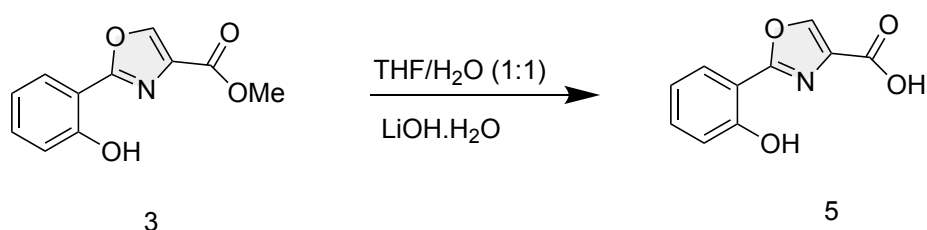


Figure 22. The synthetic route of compound **5**.

This reaction is showing hydrolysis of ester to the corresponding carboxylic acid (Kaplan and Wuest, 2021). Lithium cations were observed to accelerate the hydrolysis of esters in a water/tetrahydrofuran (THF) two-phase system (Hayashi et al., 2021).

To the solution of compound **3** (216.4 mg, 987.24 μmol) in 10 mL of THF and 10 mL of H<sub>2</sub>O was added lithium hydroxide monohydrate (124.1 mg, 2.96 mmol) and the reaction was being stirred for two hours at room temperature. Then, THF was removed under reduced pressure and the product was dissolved in 10 mL of AcOEt. After that, the mixture was acidified to pH = 2-3 with 5% HCl and extracted with AcOEt (3 x 10 mL), after which it was washed with 10 mL of saturated aqueous NaCl solution. The mixture was concentrated under reduced pressure, yielding **5** as a white solidified product (181.1 mg, 92%).

**<sup>1</sup>H NMR (300 MHz, CD<sub>3</sub>OD) δ ppm:** 8.59 (s, 1H, H9), 7.89 (d, *J* = 8.0 Hz, 1H, H3), 7.43 (t, *J* = 8.4 Hz, 1H, H5), 7.06 (d, *J* = 8.4 Hz, 1H, H6), 7.00 (t, *J* = 8.0 Hz, 1H, H4).



**$^{13}\text{C}$  NMR (75 MHz,  $\text{CD}_3\text{OD}$ )  $\delta$  ppm:** 162.39 (C, C10), 161.77 (C, C7), 157.14 (C, C1), 143.39 (CH, C9), 133.07 (CH, C2), 132.91 (CH, C5), 126.15 (CH, C3), 119.43 (CH, C4), 116.88 (C, C6), 110.13 (C, C8).

**(-)-HRMS (ESI)  $m/z$ :** 226.0110  $[\text{M}-\text{H}]^-$  (calculated for  $\text{C}_{10}\text{H}_5\text{NNaO}_4^-$ : 226.0122).

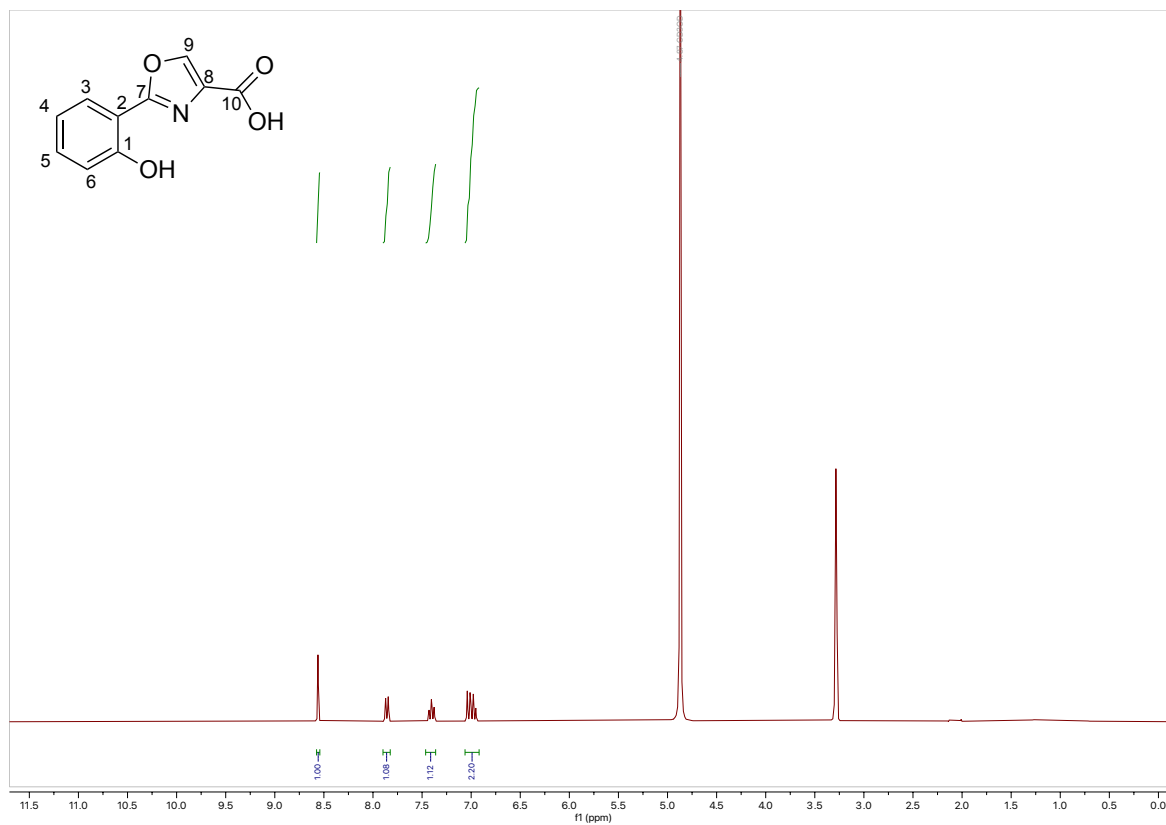


Figure 23.  $^1\text{H}$  spectrum of compound 5 in  $\text{MeOD}$ .

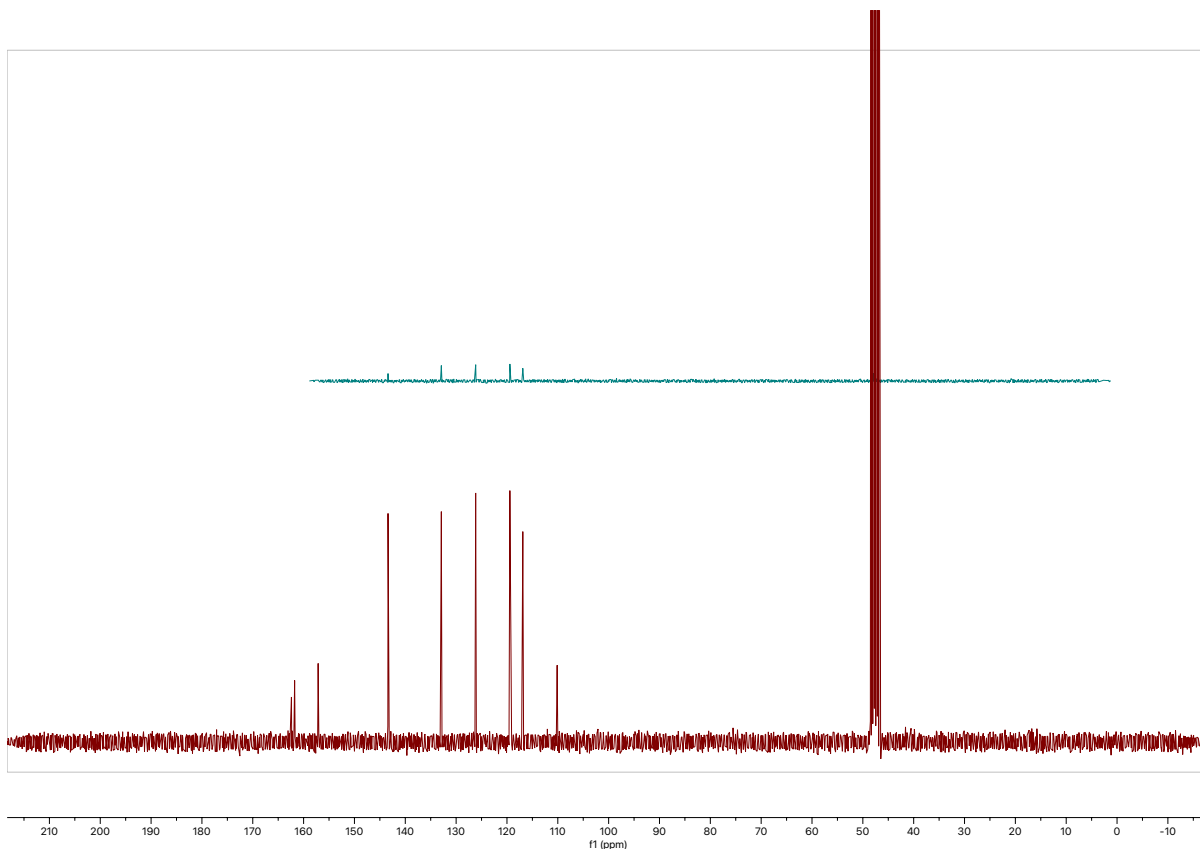


Figure 24.  $^{13}\text{C}$  spectrum of compound 5 in MeOD.

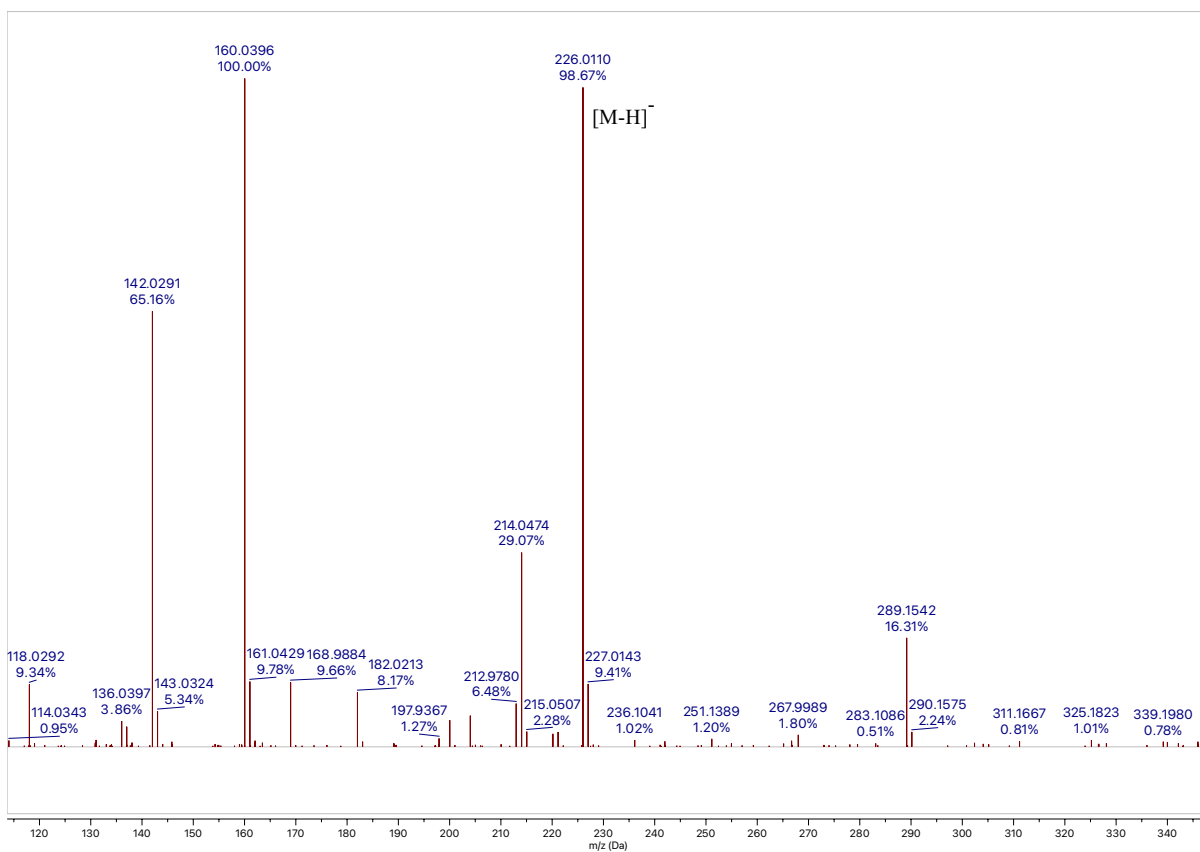


Figure 25. High-resolution MS spectrum of compound 5.

## Synthesis of compound 6

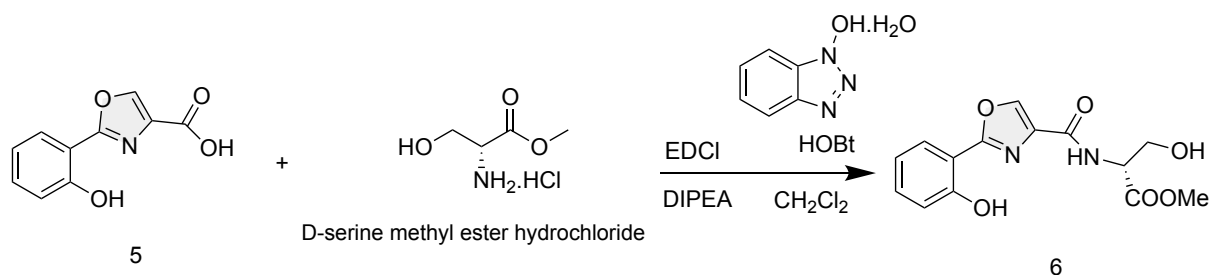


Figure 26. The synthetic route of compound 6.

The mechanism of this reaction is the same as in the reaction forming molecule 1. The only difference is that in this reaction, the oxazole ring is already present and instead of L-serine methyl ester hydrochloride, D-serine methyl ester hydrochloride was used, because it is necessary to obtain the stereochemical properties as drawn.

To the solution of compound **5** (185.2 mg, 902.67  $\mu\text{mol}$ ) in 30 mL of anhydrous  $\text{CH}_2\text{Cl}_2$ , D-serine methyl ester hydrochloride (183.0 mg, 1.18 mmol), anhydrous DIPEA (310  $\mu\text{L}$ , 1.83 mmol), EDC.HCl (190.8 mg, 995.31  $\mu\text{mol}$ ) and HOBT.H<sub>2</sub>O (207.5 mg, 1.35 mmol) were added. The reaction was done using dry conditions and was being stirred overnight at room temperature. After that,  $\text{CH}_2\text{Cl}_2$  was evaporated under reduced pressure and the product was redissolved in 20 mL of AcOEt and then washed with 10 mL of saturated aqueous  $\text{NaHCO}_3$  solution, H<sub>2</sub>O, 0.05 M HCl, H<sub>2</sub>O and saturated NaCl solution. The organic phase was dried with  $\text{MgSO}_4$ , filtered, and concentrated under reduced pressure, yielding **6** as a white solidified product (134.6 mg, 81%).

**<sup>1</sup>H NMR (300 MHz, CD<sub>3</sub>OD)  $\delta$  ppm:** 8.52 (s, 1H, H9), 7.91 (d,  $J = 7.8$  Hz, 1H, H3), 7.44 (t,  $J = 8.0$  Hz, 1H, H5), 7.07 (d,  $J = 8.0$  Hz, 1H, H6), 7.01 (t,  $J = 7.8$  Hz, 1H, H4), 4.61 (s, 1H, H11), 4.00 (qd,  $J = 11.6, 4.7$  Hz, 2H, H12), 3.79 (s, 3H, H14).

**<sup>13</sup>C NMR (75 MHz, CDCl<sub>3</sub>)  $\delta$  ppm:** 170.36 (C, C13), 167.24 (C, C10), 159.99 (C, C7), 156.99 (C, C1), 140.67 (CH, C9), 133.47 (CH, C5), 133.25 (C, C2), 126.62 (CH, C3), 120.01 (CH, C4), 117.46 (CH, C6), 110.19 (C, C8), 63.28 (CH<sub>2</sub>, C12), 54.50 (CH, C11), 53.04 (CH<sub>3</sub>, C14).

**(+)-HRMS (ESI)  $m/z$ :** 329.0475 [ $\text{M}+\text{Na}$ ]<sup>+</sup> (calculated for  $\text{C}_{14}\text{H}_{14}\text{N}_2\text{NaO}_6^+$ : 329.0744).

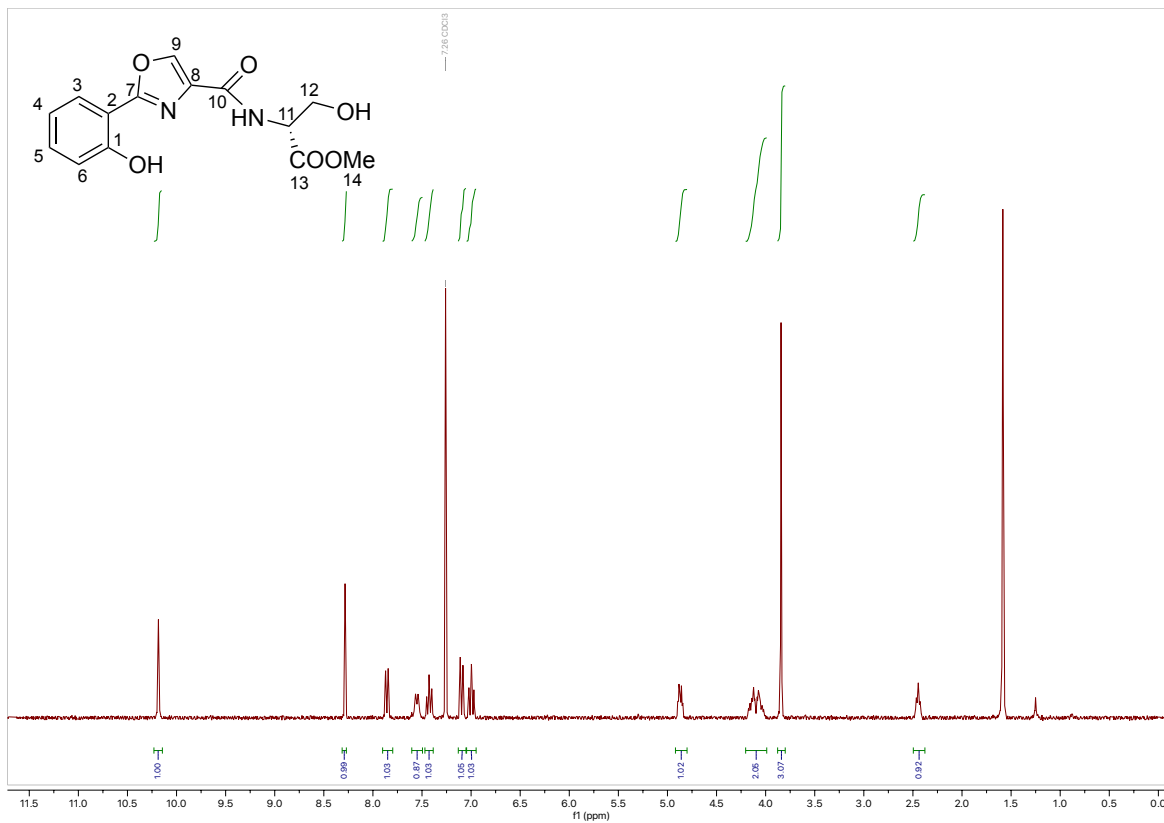


Figure 27.  $^1\text{H}$  spectrum of compound 6 in  $\text{CDCl}_3$ .

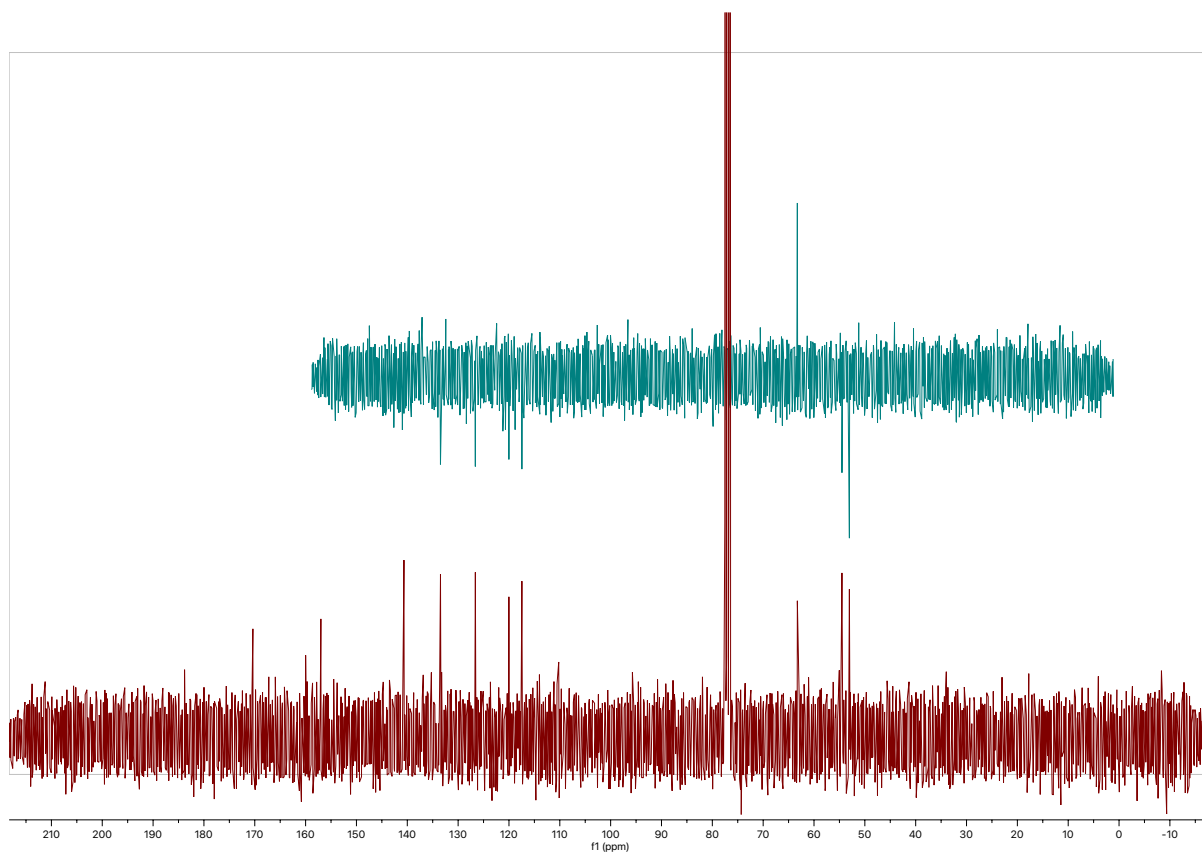


Figure 28.  $^{13}\text{C}$  spectrum of compound 6 in  $\text{CDCl}_3$ .

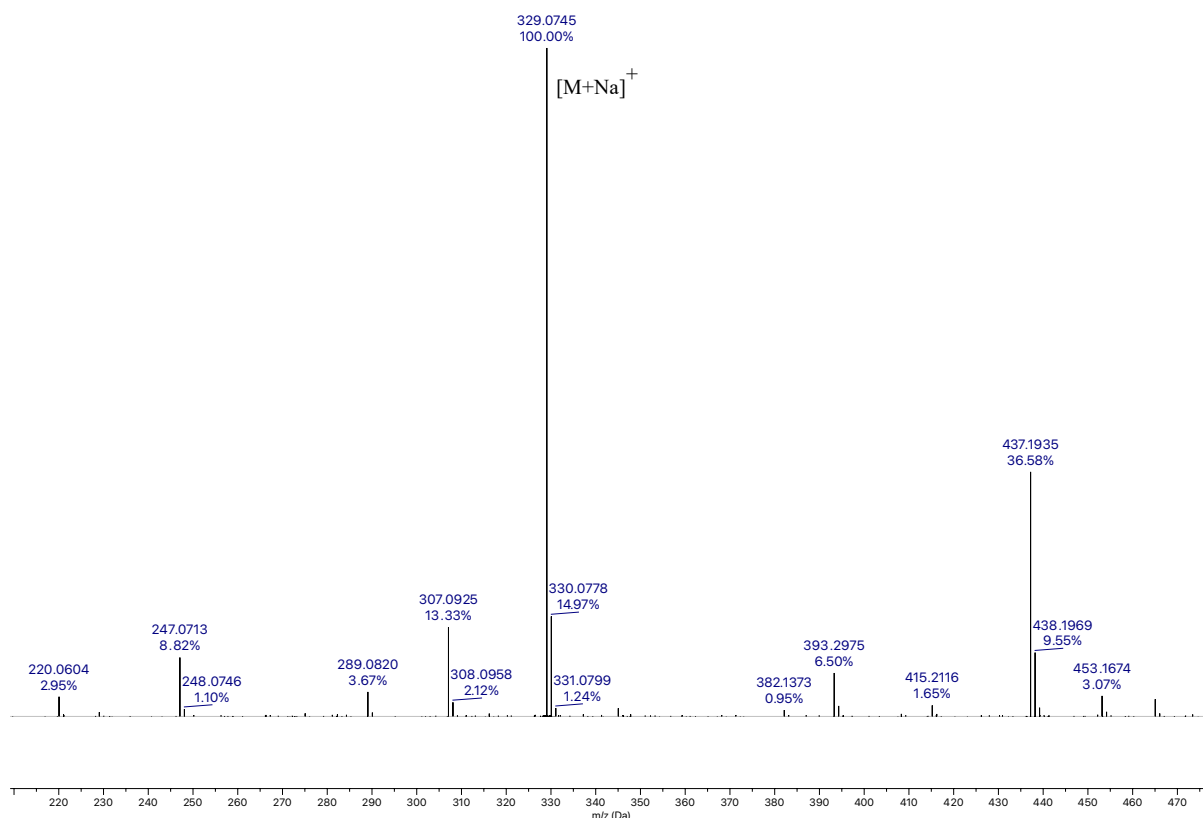


Figure 29. High-resolution MS spectrum of compound 6.

### Synthesis of compound 7

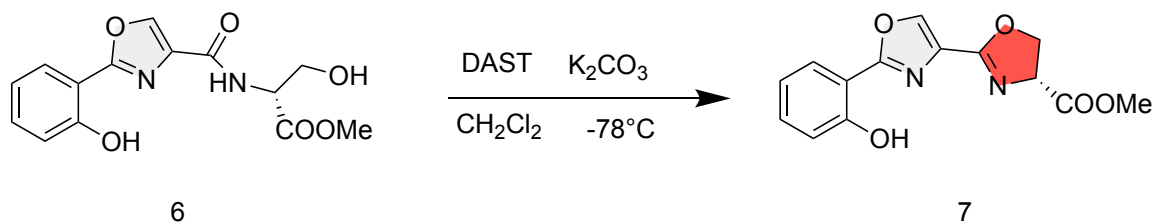


Figure 30. The synthetic route of compound 7.

The mechanism of this reaction is identical as one in the reaction forming molecule 2, this time forming a molecule with one oxazole and one oxazoline ring, which are present in the goal molecule of this project.

To the solution of compound **6** (237.9 mg, 776.76  $\mu\text{mol}$ ) in 15 mL of anhydrous  $\text{CH}_2\text{Cl}_2$ , DAST (165  $\mu\text{L}$ , 1.17 mmol) was added and the reaction was being stirred for one and a half hours at  $-78^\circ\text{C}$ . After that,  $\text{K}_2\text{CO}_3$  (162.0 mg, 1.17 mmol) was added at room temperature to quench DAST. Then, 10 mL of saturated aqueous  $\text{NaHCO}_3$  solution were added and the phases were

separated. Aqueous phase was extracted with CH<sub>2</sub>Cl<sub>2</sub> (2 x 10 mL). The organic phases were combined, washed with 10 mL of saturated aqueous NaCl solution, dried with MgSO<sub>4</sub>, filtered, and concentrated under reduced pressure, yielding **7** as a light-yellow solidified product (223.1 mg, quantitative yield).

**<sup>1</sup>H NMR (300 MHz, CDCl<sub>3</sub>) δ ppm:** 10.56 (s, 1H, H1), 8.20 (s, 1H, H9), 7.84 (d, J = 7.8 Hz, 1H, H3), 7.40 (t, J = 8.0 Hz, 1H, H5), 7.09 (d, J = 8.0 Hz, 1H, H6), 6.97 (t, J = 7.8 Hz, 1H, H4), 5.00 (dd, J = 10.6, 8.0 Hz, 1H, H11), 4.78 – 4.56 (m, 2H, H12), 3.84 (s, J = 1.1 Hz, 3H, H14).

**<sup>13</sup>C NMR (75 MHz, CDCl<sub>3</sub>) δ ppm:** 171.07 (C, C13), 162.20 (C, C10), 159.37 (C, C7), 157.46 (C, C1), 140.38 (CH, C9), 133.28 (CH, C5), 129.77 (C, C2), 126.36 (CH, C3), 119.61 (CH, C4), 117.60 (CH, C6), 110.20 (C, C8), 69.71 (CH<sub>2</sub>, C12), 68.58 (CH, C11), 52.95 (CH<sub>3</sub>, C14).

**(+)-HRMS (ESI) *m/z*:** 289.0820 [M+H]<sup>+</sup> (calculated for C<sub>14</sub>H<sub>13</sub>N<sub>2</sub>O<sub>5</sub><sup>+</sup>: 289.0824).

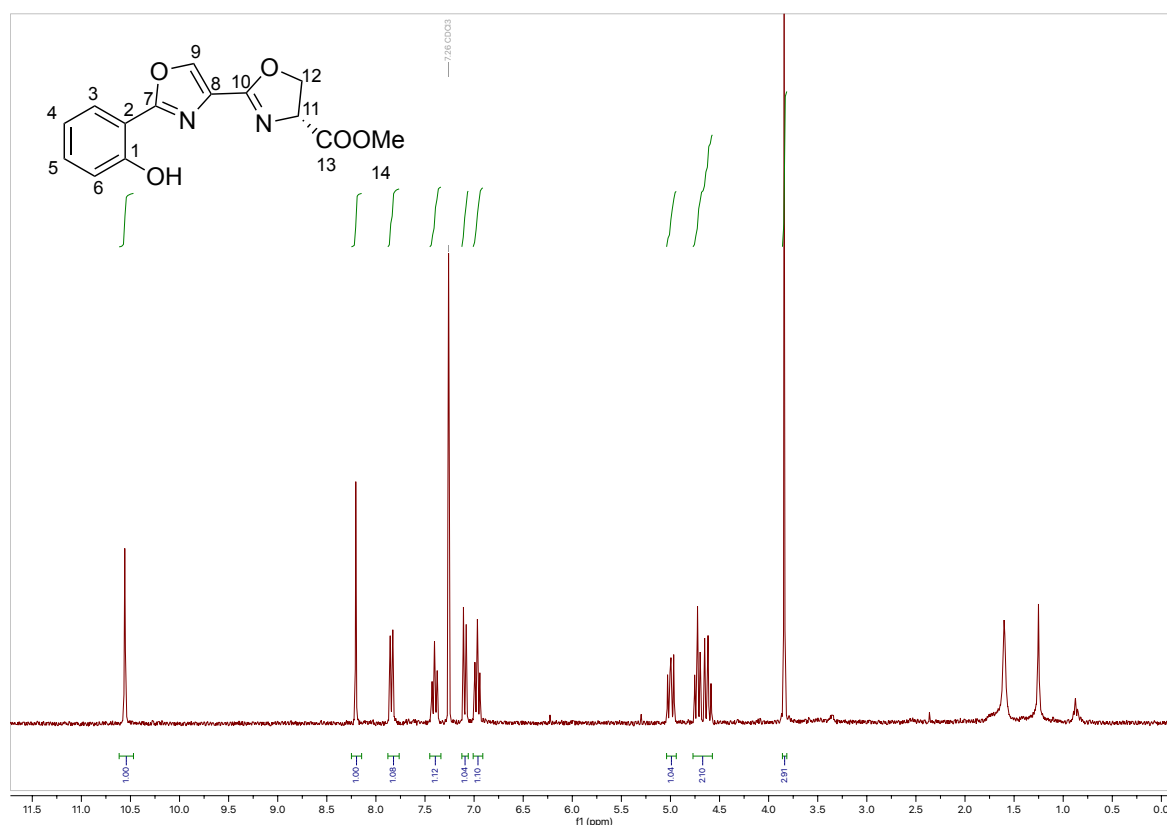


Figure 31. <sup>1</sup>H spectrum of compound **7** in CDCl<sub>3</sub>.

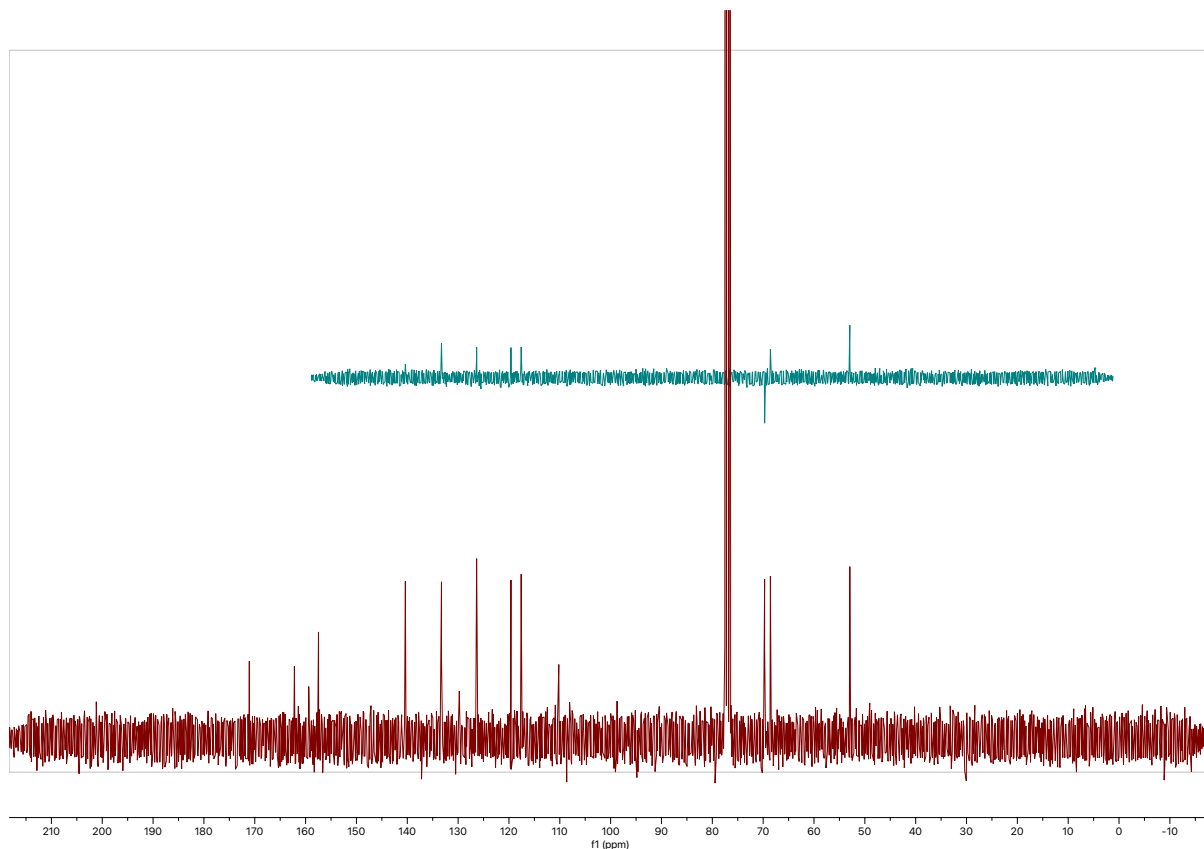


Figure 32.  $^{13}\text{C}$  spectrum of compound 7 in  $\text{CDCl}_3$ .

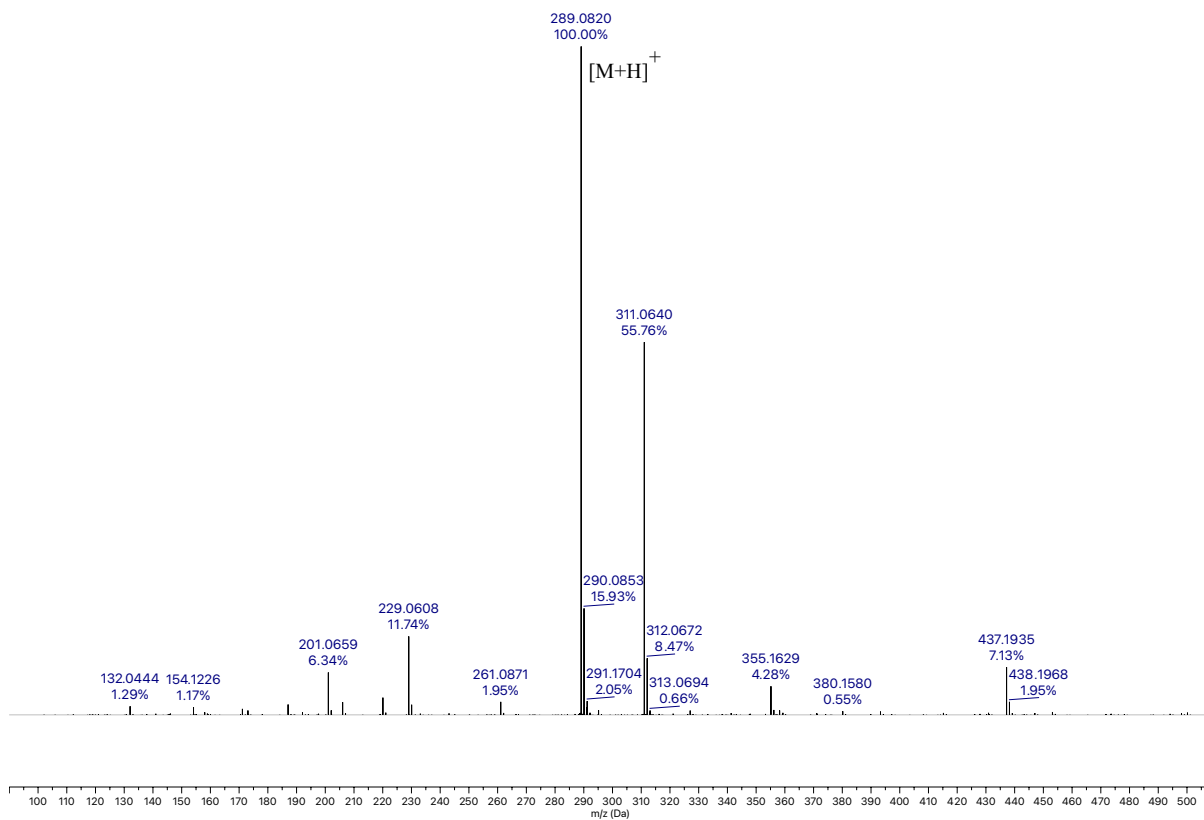


Figure 33. High-resolution MS spectrum of compound 7.

## Synthesis of compound 8

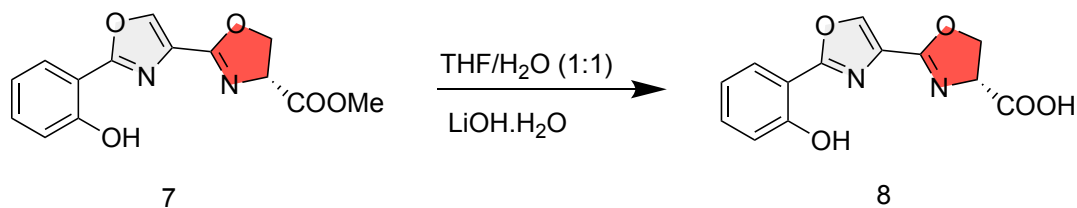


Figure 34. The synthetic route of compound 8.

The final reaction has the same mechanism as the reaction forming molecule 3, but in this reaction, the intermediate was elaborated differently. The first time this reaction was conducted, the elaboration was done the same as in the reaction of making molecule 3, but NMR signals showed that the oxazoline ring opened, probably because of the acidic conditions. The next time, HLB chromatography was used instead, and the NMR signals were satisfactory.

To the solution of compound 7 (51.7 mg, 179.35  $\mu\text{mol}$ ) in 5 mL of THF and 5 mL of  $\text{H}_2\text{O}$  was added lithium hydroxide monohydrate (16.0 mg, 381.32  $\mu\text{mol}$ ) and the reaction was being stirred for two hours at room temperature. Then, THF was removed under reduced pressure and water was eliminated using the oil pump. The solid was then purified using HLB chromatography: the cartridge was first conditioned with 6 mL of acetonitrile and 6 mL of water; the solid was then dissolved in 6 mL of water and added to the cartridge. In order were added 6 mL of water:acetonitrile mixture (3:1), 6 mL of 1:1 mixture, 6 mL of 1:3 mixture and finally 6 mL of acetonitrile. The tubes were concentrated under reduced pressure, yielding 8 as a white solidified product (49.1 mg, quantitative yield).

**$^1\text{H}$  NMR (300 MHz,  $\text{CDCl}_3$ )  $\delta$  ppm:** 8.39 (s, 1H, H9), 7.81 (d,  $J = 8.2, 1.7$  Hz, 1H, H3), 7.27 (t,  $J = 8.1$  Hz, 1H, H5), 6.88 (d,  $J = 8.1$  Hz, 1H, H6), 6.68 (t,  $J = 8.2$  Hz, 1H, H4), 4.85 – 4.65 (m, 2H, H12), 4.59 (t,  $J = 7.9$  Hz, 1H, H11).

**$^{13}\text{C}$  NMR (75 MHz,  $\text{CDCl}_3$ )  $\delta$  ppm:** 176.94 (C, C13), 168.92 (C, C10), 163.67 (C, C7), 159.13 (C, C1), 139.77 (CH, C9), 138.95 (CH, C8), 132.65 (CH, C5), 129.59 (C, C2), 127.15 (CH, C3), 119.97 (CH, C6), 102.55 (CH, C4), 71.82 (CH, C11), 70.07 (CH<sub>2</sub>, C12).

**(+)-HRMS (ESI)  $m/z$ :** 297.0483 [ $\text{M} + \text{Na}$ ]<sup>+</sup> (calculated for  $\text{C}_{13}\text{H}_{10}\text{N}_2\text{NaO}_5^+$ : 297.0482).



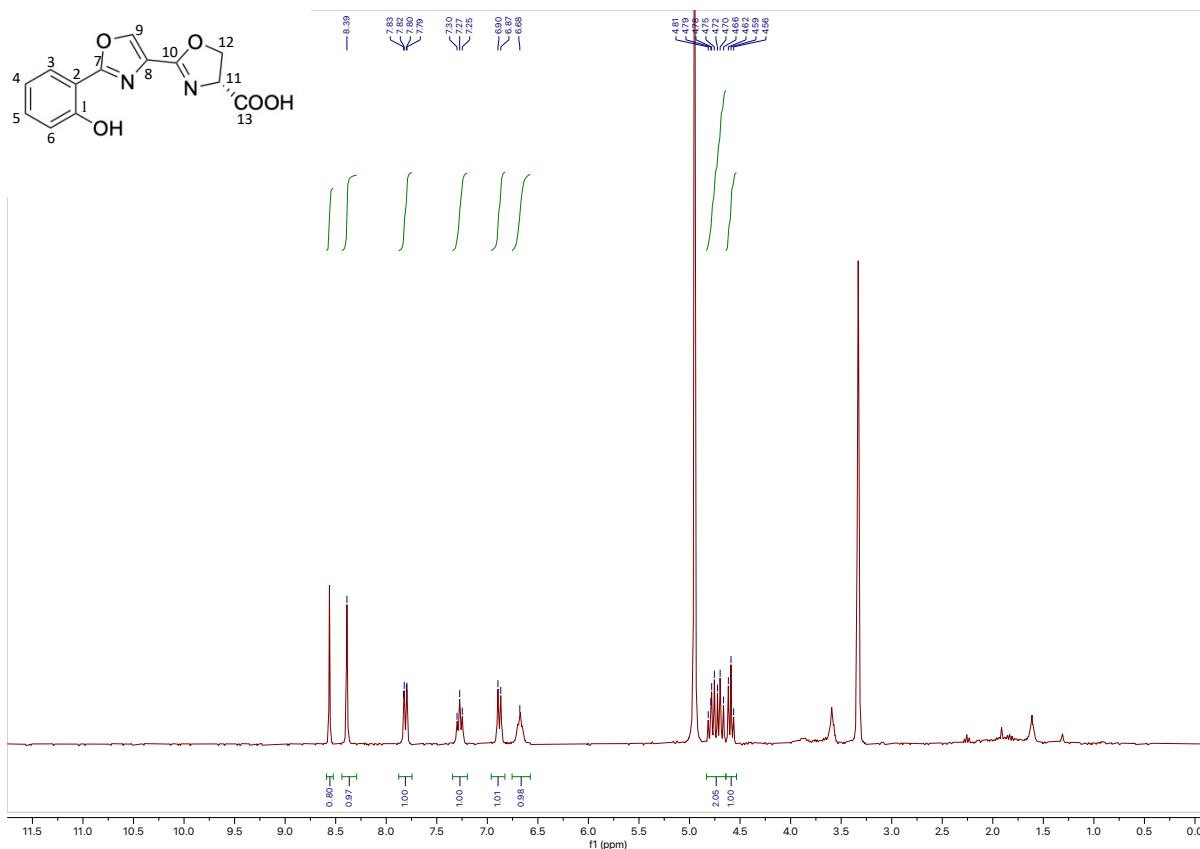


Figure 35.  $^1\text{H}$  spectrum of compound 8 in MeOD.

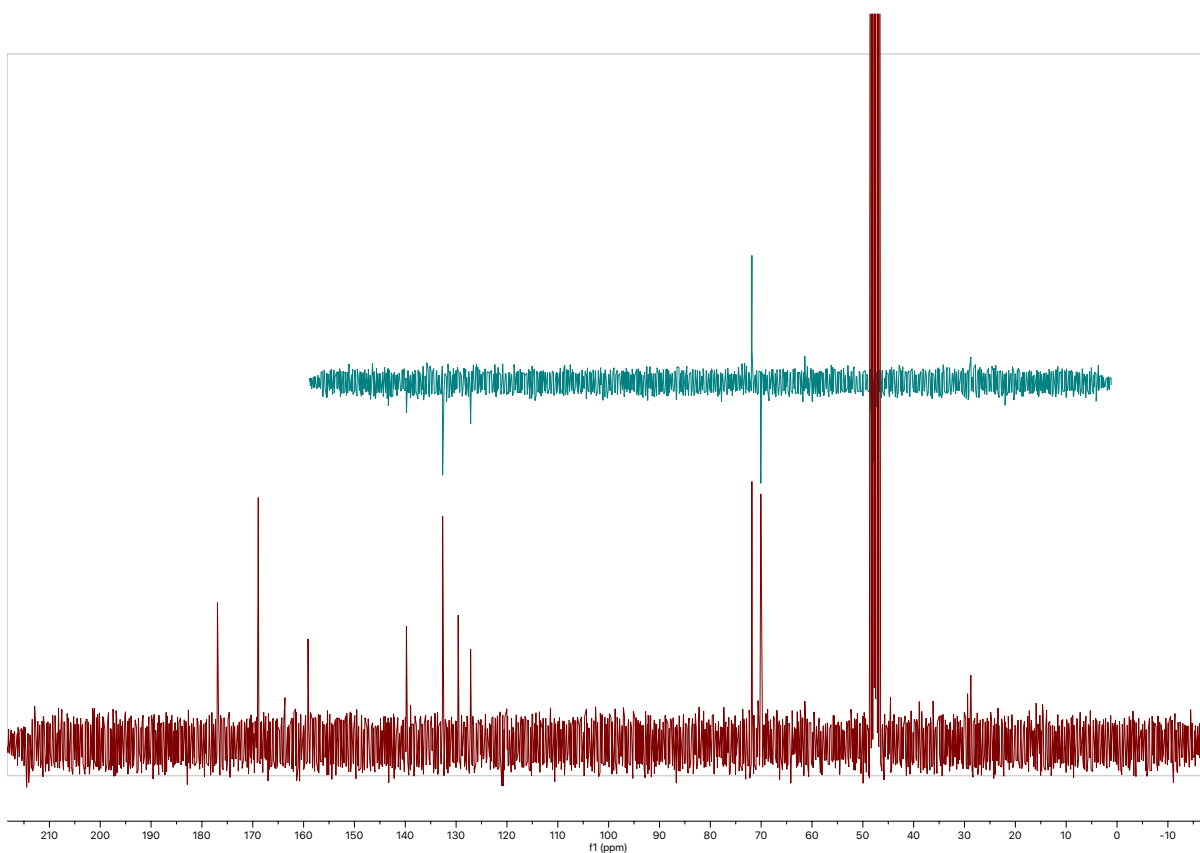


Figure 36.  $^{13}\text{C}$  spectrum of compound 8 in MeOD.

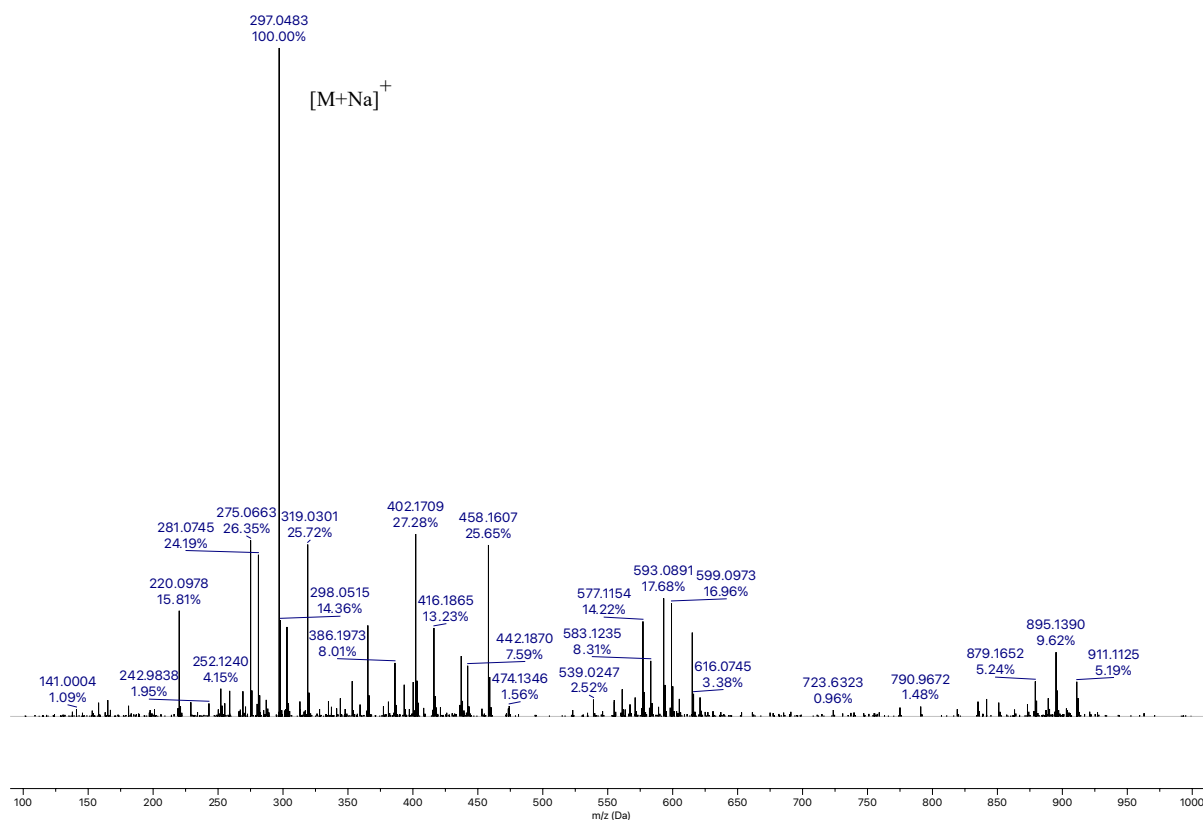


Figure 37. High-resolution MS spectrum of compound 8.

Compound 8 represents the advanced intermediate in the synthetic route of the siderophore piscibactin. It can be used for further synthesis and analysis and has the potential to benefit pharmaceutical industries and aquaculture.

## 5. CONCLUSIONS

1. Based on the proposed DFT calculation results and the theoretical complexity of the synthesis, the model with the satisfactory sum of the transverse angles and STD of atom distances was chosen.
2. The synthetic route of the O\_OZ\_T analogue was proposed, modifying some parameters from the literature to achieve high yields.
3. The preparation of an advanced intermediate was achieved, which may allow the synthesis of the simplified Pcb O\_OZ\_T analogue in the future.
4. Replacing the thiazolidine C ring of a labile nature with a more stable oxazoline ring, resulted in a more stable final molecule.
5. Removing one chiral centre from the molecule makes it easier to synthesize in the future.
6. The structures of all synthesized compounds were confirmed with high resolution mass spectra analysis and  $^1\text{H}$  and  $^{13}\text{C}$  NMR experiments.

## 6. ABBREVIATION LIST

AcCl - acetyl chloride

AcOEt - ethyl acetate

AMR - antimicrobial resistance

ATP - adenosine triphosphate

BrCCl<sub>3</sub> - bromotrichloromethane

CaH<sub>2</sub> - calcium hydride

CD<sub>3</sub>OD - deuterated methanol

CDCl<sub>3</sub> - deuterated chloroform

CH<sub>2</sub>Cl<sub>2</sub> - dichloromethane

CICA - Centro Interdisciplinar de Química e Biología; Interdisciplinary Center for Chemistry and Biology

d - doublet

DAST - diethylaminosulfur trifluoride

DBU - 1,8-Diazabicyclo[5.4.0]undec-7-ene

dd - doublet of doublets

DFT - density functional theory

T - thiazole

DIPEA - N,N-Diisopropylethylamine

DMAP - 4-Dimethylaminopyridine

DMF - dimethylformamide

DNA - deoxyribonucleic acid

dt - doublet of triplets

EDC/EDCI - 1-Ethyl-3-(3-dimethylaminopropyl)carbodiimide

ESI - electrospray ionization

FAO - Food and Agriculture Organisation

Fur - ferric uptake regulator

H<sub>2</sub>O - water

HCl - hydrochloric acid

HLB - hydrophilic–lipophilic balance

HOBt - hydroxybenzotriazole

HRMS - high-resolution mass spectrometry

J - coupling constant

$K_2CO_3$  - potassium carbonate  
Kf - formation constant  
Kps - solubility Product Constant  
LiOH - lithium hydroxide  
M - molarity  
m - multiplet  
MeOH - methanol  
MgSO<sub>4</sub> - magnesium sulphate  
MS - mass spectrometry  
NaCl - sodium chloride  
NaHCO<sub>3</sub> - sodium bicarbonate  
NMR - nuclear magnetic resonance  
NPRS - non-ribosomal peptide synthase  
O - oxazole  
OD - oxazolidine  
OZ - oxazoline  
P - pyrrolidine  
PC - pyrrolidine-cis  
Pcb - piscibactin  
PKS - polyketide synthase  
PT - pyrrolidine-trans  
qd - quartet of doublets  
s - singlet  
SAI - Servicios de Apoyo á Investigación; Research Support Service  
STD - standard deviation  
t - triplet  
TBDMS/TBDMSCl - tert-Butyldimethylsilyl  
TD - thiazolidine  
THF - tetrahydrofuran  
TLC - thin-layer chromatography  
TZ - thiazoline  
USD - United States dollars  
UV - ultraviolet  
WHO - World Health Organisation

## 7. REFERENCES

Al-Tawfiq, J.A., Ebrahim, S.M., Memish, Z.A. (2024) Preventing Antimicrobial Resistance Together: Reflections on AMR Week 2023. *J. Epidemiol. Glob. Health* [online], 14(2), 249-251. Available on: <https://doi.org/10.1007/s44197-023-00178-1> [7.7.2024.]

Balado, M., Lages, M.A., Fuentes-Monteverde, J.C., Martínez-Matamoros, D., Rodríguez, J., Jiménez, C., Lemos, M.L. (2018) The Siderophore Piscibactin Is a Relevant Virulence Factor for *Vibrio anguillarum* Favored at Low Temperatures. *Front Microbiol.* [online], 9:1766. Available on: <https://doi.org/10.3389/fmicb.2018.01766> [30.6.2024.]

Chan, K.H., Groves, J.T. (2021) Concise Modular Synthesis and NMR Structural Determination of Gallium Mycobactin T. *J. Org. Chem.* [online], 86(21), 15453-15468. Available on: <https://doi.org/10.1021/acs.joc.1c01966> [13.7.2024.]

Chiotellis, A., Selivanova, S.V., Schweizer, B., Schibli, R., Ametamey, S.M. (2014) Studies toward terminal (fluoroalkyl)silanes. Investigation of diethylaminosulfur trifluoride (DAST) in exchange reactions with some terminal (hydroxyalkyl)silanes. *Journal of Fluorine Chemistry* [online], 160, 20-28. Available on: <https://doi.org/10.1016/j.jfluchem.2013.12.011> [14.7.2024.]

De La Fuente, M.C., Ageitos, L., Lages, M.A., Martínez-Matamoros, D., Forero, A.M., Balado, M., Lemos, M.L., Rodríguez, J., Jiménez, C. (2023) Structural Requirements for Ga<sup>3+</sup> Coordination in Synthetic Analogues of the Siderophore Piscibactin Deduced by Chemical Synthesis and Density Functional Theory Calculations. *Inorganic Chemistry* [online], 62(19), 7503-7514. Available on: <https://doi.org/10.1021/acs.inorgchem.3c00787> [5.7.2024.]

De La Fuente, M.C., Segade, Y., Valderrama, K., Rodríguez, J., Jiménez, C. (2021) Convergent Total Synthesis of the Siderophore Piscibactin as Its Ga<sup>3+</sup> Complex. *Organic Letters* [online], 23(2), 340-345. Available on: <https://doi.org/10.1021/acs.orglett.0c03850> [28.6.2024]

FAO. (2023) *Fishery and Aquaculture Statistics - Yearbook 2020*. Rome: Food and Agriculture Organisation of the United Nations. Available on: <https://doi.org/10.4060/cc7493en> [27.6.2024.]

Hayashi, K., Ichimaru, Y., Sugiura, K., Maeda, A., Harada, Y., Kojima, Y., Nakayama, K., Imai, M. (2021) Efficiency of Lithium Cations in Hydrolysis Reactions of Esters in Aqueous Tetrahydrofuran. *Chemical and Pharmaceutical Bulletin* [online], 69(6), 581-584. Available on: <https://doi.org/10.1248/cpb.c21-00013> [16.7.2024.]

Hennigar, S.R., McClung, J.P. (2016) Nutritional Immunity: Starving Pathogens of Trace Minerals. *Am J Lifestyle Med.* [online], 10(3), 170-173. Available on: <https://journals.sagepub.com/doi/10.1177/1559827616629117> [2.7.2024.]

Kaplan, A.R., Wuest, W.M. (2021) Promiscuous Pseudomonas: Uptake of non-endogenous ligands for iron acquisition. *Tetrahedron Letters* [online], 75, 153204. Available on: <https://doi.org/10.1016/j.tetlet.2021.153204> [11.7.2024.]

Kramer, J., Özkaya, Ö., Kümmerli, R. (2019) Bacterial siderophores in community and host interactions. *Nat Rev Microbiol.* [online], 18(3), 152-163. Available on: <https://doi.org/10.1038/s41579-019-0284-4> [5.7.2024.]

Lages, M.A., de la Fuente, M.C., Ageitos, L., Martínez-Matamoros, D., Rodríguez, J., Balado, M., Jiménez, C., Lemos, M.L. (2022) FrpA is the outer membrane piscibactin transporter in *Vibrio anguillarum*: structural elements in synthetic piscibactin analogues required for transport. *J. Biol. Inorg. Chem.* [online], 27, 133-142. Available on: <https://doi.org/10.1007/s00775-021-01916-1> [8.7.2024.]

Lages, M.A.; Ageitos, L.; Rodríguez, J.; Jiménez, C.; Lemos, M.L.; Balado, M. (2022) Identification of Key Functions Required for Production and Utilization of the Siderophore Piscibactin Encoded by the High-Pathogenicity Island *irp*-HPI in *Vibrionaceae*. *Int. J. Mol. Sci.* [online], 23(16), 8865. Available on: <https://doi.org/10.3390/ijms23168865> [7.7.2024.]

Li, M., Ma, J.-A., Liao, S. (2023) Atom-Transfer Radical Polymerization of a SuFExable Vinyl Monomer and Polymer Library Construction via SuFEx Click Reaction. *Macromolecules* [online], 56(3), 806-814. Available on: <https://doi.org/10.1021/acs.macromol.2c01492> [16.7.2024.]

Morrison, L., & Zembower, T. R. (2020) Antimicrobial Resistance. *Gastrointestinal Endoscopy Clinics of North America* [online], 30(4), 619-635. Available on: <https://doi.org/10.1016/j.giec.2020.06.004> [7.7.2024.]

Norman, R.A., Crumlish, M., Stetkiewicz, S. (2019) The importance of fisheries and aquaculture production for nutrition and food security. *Revue Scientifique et Technique* [online], 38(2), 395-407. Available on: <https://dspace.stir.ac.uk/bitstream/1893/29935/1/1.2%20NORMAN%20postreviewversion.pdf> [28.6.2024]

Padilha, D.S., Santos, Y.F., Giacomini, L.C., Castro, F.A.V., Pereira, M.D., Rocha, A.B., Resende, J.A.L.C., Scarpellini, M. (2017) Synthesis, characterization and biological activity of gallium(III) complexes with non-symmetrical N<sub>2</sub>O-donor Schiff bases. *Polyhedron* [online], 123, 480-489. Available on: <https://doi.org/10.1016/j.poly.2016.12.020> [11.7.2024.]

Rodríguez Pedrouzo, A. (2023) *Synthetic approach of stable analogues of the siderophore piscibactin*. Master's thesis. University of A Coruña.

Sattar Jabbar, S., Al-Hamashi, A.A. (2024) The Importance of Retrosynthesis in Organic Synthesis. *Great Britain Journals Press* [online], 24 (7), 51-76. Available on: [https://journalspress.com/LJRS\\_Volume24/The-Importance-of-Retrosynthesisin-Organic-Synthesis.pdf](https://journalspress.com/LJRS_Volume24/The-Importance-of-Retrosynthesisin-Organic-Synthesis.pdf) [20.7.2024.]

Shakya, R., Peng, F., Liu, J., Heeg, M.L., Verani, C.N. (2006) Synthesis, Structure, and Anticancer Activity of Gallium(III) Complexes with Asymmetric Tridentate Ligands: Growth Inhibition and Apoptosis Induction of Cisplatin-Resistant Neuroblastoma Cells. *Inorganic Chemistry* [online], 45(16), 6263-6268. Available on: <https://doi.org/10.1021/ic060106g> [11.7.2024.]

Souto, A., Montaños, M.A., Rivas, A.J., Balado, M., Osorio, C.R., Rodríguez, J., Lemos, M.L., Jiménez, C. (2012) Structure and biosynthetic assembly of piscibactin, a siderophore from *Photobacterium damsela* subsp. *piscicida*, predicted from genome analysis. *European J. Org. Chem.* [online], 5693–5700. Available on: <https://doi.org/10.1002/ejoc.201200818> [30.6.2024.]



Wu, Y.-J., Yang, B.V. (2013) Five-Membered Ring Systems: With N and S (Se) Atoms. *Progress in Heterocyclic Chemistry* [online], 25, 257-275. Available on: <https://doi.org/10.1016/B978-0-08-099406-2.00010-8> [11.7.2024.]

## 8. SUMMARY/SAŽETAK

The fishery and aquaculture sector are being negatively impacted by a rising number of bacterial diseases in fish. Additionally, antimicrobial resistance is becoming one of the most concerning problems in the health sector globally. As a result, there is an urgent need of implementing new strategies to prevent and stop infectious diseases, as well as inventing effective antibiotics, which would help fight the resistance amongst bacteria.

Piscibactin (Pcb) is a phenolate-type siderophore, comprising two thiazoline and one thiazolidine rings. It facilitates  $\text{Fe}^{3+}$  ion uptake in bacteria, such as *Photobacterium damsela* subsp. *piscicida* and *Vibrio anguillarum*. However, its limited stability impairs the potential medical and biotechnological applications. Therefore, the development of stable Pcb analogues is crucial for further advancement.

This study proposes the design of a simplified analogue of Pcb with alternative structural features, guided by computational results.

The oxazole-oxazoline-thiazole Pcb analogue intermediate was successfully synthesised, and it could be used as an advanced intermediate in further analogue synthesis, as well as in pharmaceutical industry. All the synthesised compounds were characterised by both NMR and mass spectrometry techniques.

Rastući broj bakterijskih oboljenja u riba negativno utječe na sektor ribarstva i akvakulture. Antimikrobna rezistencija postaje jedan od najzabrinjavajućih problema u zdravstvenom sektoru diljem svijeta, rezultirajući hitnom potrebom za implementacijom novih strategija kako bi se zarazne bolesti prevenirale i zaustavile. Javlja se i potreba za izumom djelotvornih antibiotika koji bi pomogli u borbi protiv rezistencije među bakterijama.

Piscibactin (Pcb) je siderofor fenolnog tipa koji se sastoji od dva tiazolinska i jednog tiazolidinskog prstena. Olakšava unos  $\text{Fe}^{3+}$  iona u bakterije kao što su *Photobacterium damsela* subsp. *piscicida* i *Vibrio anguillarum*. Međutim, ograničena stabilnost narušava potencijalnu primjenu u medicinske i biotehnološke svrhe. Stoga je razvoj stabilnih Pcb analoga ključan za daljnji napredak.

Ovaj rad izlaže sintetski put pojednostavljenog Pcb analoga s promijenjenim strukturnim značajkama, uzevši u obzir računске rezultate.

Oksazol-oksazolin-tiazol intermedijer analoga piscibactina uspješno je sintetiziran i mogao bi služiti kao napredni intermedijer u budućoj sintezi analoga, kao i u farmaceutskoj industriji. Svi sintetizirani spojevi karakterizirani su pomoću tehnika NMR-a i masene spektrometrije.

# Temeljna dokumentacijska kartica

Sveučilište u Zagrebu  
Farmaceutsko-biokemijski fakultet  
Studij: Farmacija  
Zavod za Organsku kemiju  
A. Kovačića 1, 10000 Zagreb, Hrvatska

Diplomski rad

## SINTEZA NOVIH ANALOGA SIDEROFORA PISCIBACTINA

Karlo Andlovec

### SAŽETAK

Rastući broj bakterijskih oboljenja u riba negativno utječe na sektor ribarstva i akvakulture. Antimikrobna rezistencija postaje jedan od najzabrinjavajućih problema u zdravstvenom sektoru diljem svijeta, rezultirajući hitnom potrebom za implementacijom novih strategija kako bi se zarazne bolesti prevenirale i zaustavile. Javlja se i potreba za izumom djelotvornih antibiotika koji bi pomogli u borbi protiv rezistencije među bakterijama. Piscibactin (Pcb) je siderofor fenolnog tipa koji se sastoji od dva tiazolinska i jednog tiazolidinskog prstena. Olakšava unos  $Fe^{3+}$  iona u bakterije kao što su *Photobacterium damsela* subsp. *piscicida* i *Vibrio anguillarum*. Međutim, ograničena stabilnost narušava potencijalnu primjenu u medicinske i biotehnološke svrhe. Stoga je razvoj stabilnih Pcb analoga ključan za daljnji napredak. Ovaj rad izlaže sintetski put pojednostavljenog Pcb analoga s promijenjenim strukturnim značajkama, uzevši u obzir računске rezultate. Oksazol-oksazolin-tiazol intermedijer analoga piscibactina uspješno je sintetiziran i mogao bi služiti kao napredni intermedijer u budućoj sintezi analoga, kao i u farmaceutskoj industriji. Svi sintetizirani spojevi karakterizirani su pomoću tehnika NMR-a i masene spektrometrije.

Rad je pohranjen u Središnjoj knjižnici Sveučilišta u Zagrebu Farmaceutsko-biokemijskog fakulteta.

Rad sadrži: 48 stranica, 37 grafičkih prikaza, 3 tablice i 22 literaturna navoda. Izvornik je na engleskom jeziku.

Ključne riječi: piscibactin, siderofor, O\_OZ\_T analog, računalni izračuni

Mentor: **Dr. sc. Valerije Vrčec**, redoviti profesor Sveučilišta u Zagrebu Farmaceutsko-biokemijskog fakulteta.  
**Dr. sc. Jaime Rodríguez González**, redoviti profesor Sveučilišta u A Coruñi Prirodoslovnog fakulteta

Ocjenjivači: **Dr. sc. Valerije Vrčec**, redoviti profesor Sveučilišta u Zagrebu Farmaceutsko-biokemijskog fakulteta.  
**Dr. sc. Ivana Perković**, izvanredni profesor Sveučilišta u Zagrebu Farmaceutsko-biokemijskog fakulteta.  
**Dr. sc. Davor Šakić**, docent Sveučilišta u Zagrebu Farmaceutsko-biokemijskog fakulteta.

Rad prihvaćen: rujan 2024.

## Basic documentation card

University of Zagreb  
Faculty of Pharmacy and Biochemistry  
Study: Pharmacy  
Department of Organic Chemistry  
A. Kovačića 1, 10000 Zagreb, Croatia

Diploma thesis

### SYNTHESIS OF NEW ANALOGUES OF THE SIDEROPHORE PISCIBACTIN

Karlo Andlovec

#### SUMMARY

The fishery and aquaculture sector are being negatively impacted by a rising number of bacterial diseases in fish. Additionally, antimicrobial resistance is becoming one of the most concerning problems in the health sector globally. As a result, there is an urgent need of implementing new strategies to prevent and stop infectious diseases, as well as inventing effective antibiotics, which would help fight the resistance amongst bacteria. Piscibactin (Pcb) is a phenolate-type siderophore, comprising two thiazoline and one thiazolidine rings. It facilitates  $\text{Fe}^{3+}$  ion uptake in bacteria, such as *Photobacterium damsela* subsp. *piscicida* and *Vibrio anguillarum*. However, its limited stability impairs the potential medical and biotechnological applications. Therefore, the development of stable Pcb analogues is crucial for further advancement. This study proposes the design of a simplified analogue of Pcb with alternative structural features, guided by computational results. The oxazole-oxazoline-thiazole Pcb analogue intermediate was successfully synthesised, and it could be used as an advanced intermediate in further analogue synthesis, as well as in pharmaceutical industry. All the synthesised compounds were characterised by both NMR and mass spectrometry techniques.

The thesis is deposited in the Central Library of the University of Zagreb Faculty of Pharmacy and Biochemistry.

Thesis includes: 48 pages, 37 figures, 3 tables and 22 references. Original is in English language.

Keywords: piscibactin, siderophore, O\_OZ\_T analogue, computational calculations

Mentor: **Valerije Vrčec, Ph.D.** *Full Professor*, University of Zagreb Faculty of Pharmacy and Biochemistry  
**Jaime Rodríguez González, Ph.D.**, *Full Professor*, University of A Coruña Faculty of Science

Reviewers: **Valerije Vrčec, Ph.D.** *Full Professor*, University of Zagreb Faculty of Pharmacy and Biochemistry  
**Ivana Perković, Ph.D.** *Associate Professor*, University of Zagreb Faculty of Pharmacy and Biochemistry  
**Davor Šakić, Ph.D.** *Assistant Professor*, University of Zagreb Faculty of Pharmacy and Biochemistry

The thesis was accepted: September 2024.